

# **Contemporaneous Appearances of Local-Scale Auroral Spiral and Global-Scale Transpolar Arc: Changes of Auroras and Field-Aligned Current Profiles Before a Substorm and After Its Recovery Phase**

**Motoharu Nowada<sup>1†</sup>, Yukinaga Miyashita<sup>2,3</sup>, Aoi Nakamizo<sup>4</sup>,  
Noora Partamies<sup>5</sup>, and Quan-Qi Shi<sup>1</sup>**

<sup>1</sup> Shandong Key Laboratory of Optical Astronomy and Solar-Terrestrial Environment, School of Space Science and Physics, Institute of Space Sciences, Shandong University, Weihai, Shandong, People's Republic of China.

<sup>2</sup> Korea Astronomy and Space Science Institute, Daejeon, South Korea.

<sup>3</sup> Korea University of Science and Technology, Daejeon, South Korea.

<sup>4</sup> National Institute of Communication and Technology, Koganei, Tokyo, Japan.

<sup>5</sup> Department of Arctic Geophysics, The University Centre in Svalbard, Longyearbyen, Norway

<sup>†</sup>Corresponding author: Motoharu Nowada (moto.nowada@sdu.edu.cn)

## **Key Points:**

1. After the substorm recovery phase, a nightside distorted transpolar arc and the auroral spiral can appear simultaneously.
2. Auroral spiral cannot be treated within the magnetohydrodynamics framework, but their formation is closely related to some kinetic process.
3. The transpolar arc could not be formed in magnetohydrodynamic simulations when it appeared simultaneously with the auroral spiral.

## **Running Title: Concomitance of Auroral Spiral and TPA**

**Keyword:** Transpolar arc; Auroral spiral; Field-aligned currents, Substorm, Magnetohydrodynamic simulations; Kinetic effects

## **Abstract**

Local vortex-structured auroral spiral and a large-scale transpolar arc (TPA) were contemporaneously observed by the Polar ultraviolet imager (UVI), when a substorm almost recovered. The TPA grew along the dawnside auroral oval from the nightside to the dayside (oval-aligned TPA), and a chain of multiple auroral spots and spiral were located azimuthally near the poleward edge of the nightside auroral oval. Contemporaneous appearances of the TPA and the auroral spiral can be seen after the spiral appeared alone. Polar also detected the oval-aligned TPA and another dawnside TPA with the nightside end distorted toward the premidnight sector (J-shaped TPA) before and after the spiral's formation, respectively. To examine these associated magnetotail structures, we performed global magnetohydrodynamic (MHD) simulations, based on two different types of code, BAT-S-RUS and improved REPPU, and examined how the field-aligned current (FAC) profiles varied in association with changes of the auroral form to TPA and/or auroral spiral. Global MHD simulations with the two different types of code can reproduce the TPAs and the associated FAC structures in the magnetotail. The auroral spiral and its nightside FAC profile, however, were not formed in both simulations, suggesting that its formation process cannot be treated within an MHD framework but is closely related to some kinetic process. When the J-shaped TPA and the auroral spiral contemporaneously appeared, the two MHD simulations could not reproduce the TPA, spiral and their associated magnetotail FAC structures, also advocating that a kinetic effect related to the spiral formation might prevent the TPA occurrence.

## **Plain Language Summary**

The auroral spiral, local-scale vortex-structured auroral phenomenon, and global-scale transpolar arc (TPA) bridging the polar cap between the nightside and dayside sectors of the auroral oval have been discussed to understand how the physical processes occurring in the magnetotail can be relevant to their formations within a framework of solar wind-magnetosphere-ionosphere coupling system. In this study, we find that the TPA appears prior to and after the auroral spiral, and sometimes the spiral and TPA were concomitant. Based on magnetohydrodynamic (MHD) computer simulations with two different types of simulation code, we tried to reproduce and investigate concomitance of TPA and auroral spiral and the associated field-aligned current (FAC) structures on the magnetic equatorial plane of the nightside magnetosphere. The TPA prior to and after the spiral and the associated FAC profile can be reproduced by global MHD computer

simulations, but the auroral spiral and its magnetotail FACs cannot. Even when the spiral and the TPA were concomitant, neither of the auroras can be formed in the MHD simulations, suggesting that auroral spiral formation might not be addressed within an MHD framework but would closely be related with some kinetic process.

## 1. Introduction

The auroral phenomena that locally exhibit a vortex structure and mainly appear as azimuthally-aligned spot emissions in the poleward region of the nightside auroral oval are referred to as auroral spiral (e.g., Elphinstone et al., 1995; Nowada et al., 2023; Partamies et al., 2001a). The auroral spirals were distributed over the nightside ionosphere from 18 h to 5 h magnetic local time (MLT), while their magnetic latitude (MLat) was concentrated around  $65^\circ$  (Partamies et al., 2001a) and/or between  $70^\circ$  and  $80^\circ$  (Davis and Hallinan, 1976). Statistical diameter distributions of the auroral spirals are generally 25-75 km (Partamies et al., 2001a, 2001b), or 20-1,300 km (Davis and Hallinan, 1976). Recently, it has been reported that the auroral spiral appeared during various substorm phases: expansion phase (Keiling et al. 2009a, 2009b) and late substorm recovery phase (Nowada et al. 2023). Depending on the substorm phase of spiral occurrence, the fundamental spiral features, such as its scale, duration, and formation mechanism, should be different (e.g., Nowada et al. 2023). Keiling et al. (2009a, 2009b) examined auroral spirals that occurred from the substorm onset to the expansion phase, and estimated its scale at 200-300 km. In contrast, the auroral spiral observed during the late stage of the substorm recovery phase had smaller core scale from 150 to 250 km (Nowada et al., 2023).

In the early days of auroral spiral studies, Davis and Hallinan (1976) and Hallinan and Davis (1970) showed that in addition to the spiral, curl- and fold-type auroras were accompanied by vortex structures. Spirals are the auroral phenomena with the largest vortex whose scale is larger than 50 km. Curls are small-scale auroral phenomena with vortices of less than 10 km, which are embedded in auroral arcs. Folds are distorted arcs with an intermediate scale of about 20 km. These vortical auroras, however, can appear contemporaneously in the same auroral form and could not be easily distinguished. Recently, based on the Polar ultraviolet imager (UVI) and all-sky camera imager data, Nowada et al. (2023) followed the auroral spiral formation process after substorm-associated auroral bulge distributed azimuthally in the nightside ionosphere subsided. After the substorm entered the recovery phase, several poleward-elongated auroral stream structures appeared in the nightside auroral oval. Finally, the auroral spiral was formed during the late stage of the substorm recovery phase. Nowada et al. (2023) also estimated the source region of the auroral spiral on the nightside magnetotail equatorial plane using an empirical magnetic field model. They, however, could not physically reveal how the spiral was formed, based on the

relations with the solar wind conditions and the corresponding magnetotail processes.

At present, the formation mechanism of the auroral spiral remains unclear. Keiling et al. (2009b) and Voronkov et al. (2000) proposed that the spiral might be formed by shear flow ballooning instability which is treated within a magnetohydrodynamic (MHD) regime and is driven by a pressure gradient in the magnetotail. Furthermore, the auroral spiral formation cannot be yet addressed from the viewpoint of solar wind-magnetosphere-ionosphere coupling system. Lysak and Song (1996), however, proposed a spiral formation model based on magnetosphere-ionosphere coupling within a magnetohydrodynamics (MHD) scheme. The current sheet instability (CSI) in the nightside ionosphere plays a crucial role in formation of the auroral spiral. CSI is quite similar to the Kelvin-Helmholtz instability (KHI) caused by a velocity shear, but a magnetic shear generated by an upward (from the ionosphere to the magnetosphere) field-aligned current (FAC) plays a significant role in its growth. Lysak and Song (1996) concluded that an auroral spiral can be formed by CSI because of the conductance difference between the ionosphere and the magnetosphere. Hallinan (1976) and Partamies et al. (2001b) also pointed out that enhancement of an upward FAC filament structure drives the magnetic shear and the resulting CSI to form the auroral spiral. Although the two groups of Lysak and Song (1996), and Hallinan (1976) and Partamies et al. (2001b) independently proposed the models to explain the auroral spiral formation, they all emphasized that the CSI due to an upward FAC is the major mechanism of the auroral spiral formation. At present, however, we do not have the observational evidence for their models and the CSI reproductions, based on global-scale computer simulations using MHD code, suggesting that the auroral spiral features, including the formation process, cannot yet be explained completely within the MHD regime.

Transpolar arc (TPA) is a “crossbar” type auroral phenomenon bridging the polar cap from the nightside to the dayside auroral oval and is also a part of  $\theta$ -like-shaped aurora (theta aurora). The formation process and fundamental physical features of TPA have been investigated and discussed (see reviews by Fear and Milan, 2012a, 2012b) since a theta aurora was detected by the Dynamics Explorer (DE) 1 spacecraft (Frank et al., 1982). As a representative TPA formation model, Milan et al. (2005) built a formation model based on nightside magnetic reconnection, which successfully explained the formations in several TPA cases (Fear and Milan, 2012a, 2012b; Kullen et al. 2015; Nowada et al. 2018, and references therein). The development of TPA from the nightside to the dayside poleward edge of the auroral oval can be explained by continuous formation of newly

closed field lines generated by nightside reconnection retreating its site toward the farther tail. Nowada et al. (2020) proposed a possible formation model of the dawnside (duskside) TPA whose nightside end gets distorted toward premidnight (postmidnight) sector, nightside distorted (J- and L-shaped) TPAs. They concluded that the source of the nightside distorted TPAs is FACs induced by the plasma velocity shear between a fast plasma flow caused by nightside magnetic reconnection and the slower background magnetotail plasma flow. The conventional TPA has a straight bar shape which connects the nightside and dayside sectors of the auroral ovals, but significant distortions at the nightside end as seen in the J (L)-shaped TPA comes from significant magnetic field line twisting and magnetotail deformation due to the IMF- $B_Y$  component which had already been revealed by many researchers (e.g., Cowley, 1981, 1994; Gosling et al. 1990; Tsyganenko and Fairfield, 2004; Tsyganenko and Sitnov, 2005; Tsyganenko et al. 2015).

Many researches successfully reproduced TPAs, based on global MHD simulations (e.g., Kullen and Janhunen, 2004; Tanaka et al., 2004; Watanabe et al., 2014; and references therein). This suggests that an auroral phenomenon of TPA itself can be treated and discussed within an MHD framework. TPA is actually identified as global-scale aurora because it connects dayside and nightside polar cap regions, and has significant conjugacy between the Northern and Southern Hemispheres (e.g., Carter et al. 2017; Nowada et al., 2020).

In this study, we examined a unique case observed by the Polar UVI on 10 January 1997 that the auroral morphologies temporally and drastically changed before and after a substorm. Before the substorm growth phase, the TPAs aligned with the dawnside auroral oval were observed. Even though the substorm headed for complete recovery, the auroral morphology drastically changed; that is, a nightside distorted TPA (J-shaped TPA) appeared and remained, and even auroral spiral appeared simultaneously. In particular, focusing on the interval of contemporaneous appearances of the local-scale auroral spiral and the global-scale J-shaped TPA, we examined how associated magnetotail structures were varying and how detailed ionospheric FAC profiles were, and argued how the auroral spiral and the TPA are physically related, based on two different global MHD simulations, together with the Polar UVI observations.

The instrumentation is described in Section 2. In Section 3, we show the solar wind conditions, the results of the Polar UVI observations and global MHD simulations based on two different types of code, and the comparison between the observations and the simulations. The summary and discussion of this study are described in Section 4. Finally, we described the conclusions of this

study in Section 5.

## **2. Instrumentation of the Ultraviolet Auroral Imager**

The ultraviolet imager (UVI) onboard Polar, which was launched on 24 February 1996, provides global auroral imaging data in ultraviolet range (Torr et al., 1995). We used the UVI images in altitude adjusted corrected geomagnetic (AACGM; Baker and Wing, 1989) and geographic coordinates. The UVI image data are degraded in the direction perpendicular to the track of Polar by the satellite's wobble motion (e.g., Parks et al., 1997). Because this wobble is, however, predictable (Parks et al., 1997), we used the UVI image data from which the wobble effects were mostly removed.

## **3. Results**

### **3-1. An Overview of Observation**

Figure 1 shows a fine example of the auroral spiral (pointed out with a thick yellow arrow) and the nightside distorted transpolar arc (J-shaped TPA) contemporaneously observed by the Polar UVI (panels a and b) and the all-sky camera (ASC) installed at the Longyearbyen station ( $75.32^\circ$  magnetic latitude and  $111.0^\circ$  magnetic longitude, Figure 1c) at 21:08 UT on 10 January 1997. The long-term movie of the auroral spiral detected by the Longyearbyen ASC is available in the supporting information of Nowada et al. (2023). The auroral spiral clearly identified by both Polar UVI and the Longyearbyen ASC was only one (pointed out with thick orange arrows). We, hereafter, discuss this auroral spiral identified by satellite- and ground-based observations, and the other auroral signatures azimuthally neighboring on the auroral spiral are referred to as auroral spots (auroral spiral and spots). The auroral spiral was seen to the southwest region of Svalbard Island (Figures 1b and 1c). The dawnside TPA had a nightside end distorted toward the midnight sector, and extended from the poleward edge of the postmidnight auroral at  $\sim 1$ h MLT and  $\sim 72^\circ$  MLat to the prenoon auroral oval across the dawnside of the north pole (Figure 1b; see also the supporting information of Nowada et al., 2023). This type of TPA is referred to as J-shaped TPA (see Nowada et al., 2020).

### **3-2. Solar Wind Conditions**

Figure 2 shows the OMNI solar wind parameters and geomagnetic indices for the 6 h interval

between 17:00 UT and 23:00 UT on 10 January 1997. From top to bottom, the panels show the *SMU* and *SML* indices (Newell and Gjerloev., 2011), the Y and Z components of the interplanetary magnetic field (IMF- $B_y$  and  $-B_z$ ) in geocentric solar magnetospheric (GSM) coordinates, the IMF clock angle derived with  $\arctan(\text{IMF-}B_y/\text{IMF-}B_z)$ , the Akasofu-Perreault parameter ( $\epsilon_{AP}$ , a measure of the solar wind energy input rate; Perreault and Akasofu, 1978), and the solar wind dynamic pressure ( $P_d$ ), velocity ( $V_{sw}$ ), and proton density ( $N_p$ ). The values of  $K_p$  are shown at the bottom of the figure. The intervals of the transpolar arc (growing to the dayside sector aligned with the dawnside auroral oval, oval-aligned TPA; denoted by TPA at the top of Figure 2), the auroral spiral (AS), the contemporaneous appearances of the J-shaped TPA and the auroral spiral (J-TPA+AS), and the J-shaped TPA (J-TPA) were identified by visual inspection, based on the images from Polar UVI and the all-sky camera (ASC) at the Longyearbyen station. Again, note that AS denotes only the auroral spiral that could be identified by both satellite- and ground-based observations. Each time interval is bracketed a pair of broken cyan, black, violet, or yellow lines. The detailed durations of these auroral signatures and the corresponding polarities of the IMF- $B_z$  component are also summarized in Table 1.

During this interval, the whole cycle of a substorm from onset to recovery phases, which was accompanied by moderate geomagnetic disturbances with a  $K_p$  range from 3+ to 4, can be seen. Namely, *SML* shows a sharp, large decrease from  $\sim 18:50$  UT (the substorm onset) to  $\sim 19:05$  UT, and then *SML* recovered to  $\sim 0$  nT at  $\sim 22:15$  UT. Small negative bay variations were seen in *SML* during the time intervals of AS and J-TPA+AS. On the contrast, *SMU* was almost constant during the presented time interval.

During the J-TPA+AS interval, clear jumps were seen in the IMF- $B_y$  and  $-B_z$  components, and the IMF clock angle at 21:10 UT. In particular, the IMF- $B_z$  component, which remained weakly southward for at least 4 h, showed a sharp polarity change from southward (negative) to northward (positive), while IMF- $B_y$  had a dominantly dawnward (negative) component, that is, the sign changes were not seen. Due to this abrupt IMF- $B_z$  jump, the IMF clock angle increased from  $-90^\circ$  to  $-45^\circ$ . The  $\epsilon$  parameter shows a significant decrease, associated with the clock angle's jump, which was preceded by a gradual decrease after the oval-aligned TPA disappeared. During the other auroral intervals, significant changes of the IMF, the IMF clock angle, and the solar wind plasma parameters were absent, although small excursions in the solar wind were seen. Taking a look at the solar wind conditions and the corresponding auroral morphologies, all TPA-type arcs



and auroral spiral were observed even when no significant perturbations of *SML* and *SMU* occurred.

### **3-3. Comparison of Polar UVI Auroral Observations with Magnetohydrodynamic (MHD) Simulations in the Polar Cap**

Figure 3 shows representative examples of the oval-aligned TPA, the auroral spiral, contemporaneous appearances of the J-shaped TPA and the spiral, and the J-shaped TPA that were detected by the Polar UVI (Figures 3a to 3d), and contour plots of the ionospheric conductance determined by the corresponding magnetotail processes that were reproduced by the improved REProduce Plasma Universe (REPPU) code (Tanaka, 1994; Nakamizo et al., 2009; Figures 3e to 3h). The improved REPPU code applies a grid system with angularly unstructured and increasing radial spacing. The computation using this grid system is more effectively stabilized than the other codes, that is, the solutions are hard to diverge, because there is no apparent singularity. Hence, we can expect that the structures of the global-scale TPA and the local-scale spiral are expected to be reproduced in such a grid system. According to Nakamizo et al. (2009), in the improved REPPU code, the order number of grid splitting can be increased/decreased freely, depending on the systems discussed. Changing the order number for grid splitting, we can perform the computations with higher temporal and spatial resolutions. In this MHD simulation, the ionospheric conductance can be used as a proxy of the FAC intensity.

Figures 3a – 3d are long Lyman-Birge-Hopfield emission (LBHL;  $\sim 170$  nm) images from Polar UVI with an integration time of 36 s in the same format as Figures 1a. Polar detected the TPA growing from the poleward edge of the nightside auroral oval near 3h MLT to the dayside, which was also aligned with the dawnside auroral oval (Figure 3a). This TPA was stable and had no significant dawn-dusk motion within the polar cap. Such a static TPA near the dawn (or dusk) auroral oval, so-called oval-aligned arc, had already been reported and its fundamental characteristics, such as the relation to the IMF orientations, was discussed by Murphree and Cogger (1981) and Kullen et al. (2002, 2015). The reproduction of the oval-aligned TPA, based on the improved REPPU MHD simulation can be clearly seen in Figure 3e, suggesting that the oval-aligned TPA and the associated field-aligned structure in the magnetotail can be addressed in an MHD regime.

In Figure 3b, azimuthally-chained four auroral spots, including an auroral spiral identified by the Longyearbyen all-sky camera (Nowada et al., 2023), were seen at the poleward edge of the

nightside auroral oval, but they were not reproduced by the MHD simulation as shown in Figure 3f. Even during the concomitant interval of the auroral spiral and spots, and J-shaped TPA (Figure 3c), the auroral spiral and spots were not reproduced at the poleward edge of the nightside auroral oval (Figure 3g). This result suggests that the auroral spiral might not be reproduced within an MHD framework. Interestingly, for this event, not only the spiral but also the J-shaped TPA that should be treated in an MHD regime were not reproduced by the simulation. Comparison of Figure 3d with Figure 3h supports that the J-shaped TPA is a phenomenon which can be discussed within an MHD scale. From these observations and global MHD simulations, we suggest that when the spiral and the TPA appear contemporaneously, the auroral spiral might impact on the formation process of the TPA basically discussed within an MHD framework.

### **3-4. Magnetotail Source Regions of Auroral Spiral and TPA: Polar Observations and MHD Simulations**

To investigate the source regions of the TPA and the auroral spiral in the nightside magnetosphere, we mapped each pixel data of the Polar UVI images onto the magnetic equatorial plane, based on the Tsyganenko 96 empirical magnetic field model (T96; Tsyganenko and Stern, 1996). The technical details on mapping are described in Nowada et al. (2023). Figure 4 shows the projections of the Polar UVI images of the oval-aligned TPA (Figure 4a, highlighted with a magenta broken oval), the auroral spiral (Figure 4b), and the J-shaped TPA (Figure 4c, surrounded with an orange broken curve) onto the GSM-X-Y nightside magnetic equatorial plane. Figures 4d–4f show the Polar UVI plots in the nightside ionosphere from 18 h to 6 h MLT. Note that the nightside equatorial plane mapping of the auroral images sensitively depends on magnetic field models (Lu et al., 2000).

Based on the mapping onto the magnetic equatorial plane, the source regions of the oval-aligned TPA had the structures elongating tailward to  $\sim 55 R_E$  at  $Y \sim 11 R_E$  to  $12 R_E$  (in GSM), as shown with a magenta broken oval in Figure 4a. It is interesting that the oval-aligned TPA's source region lay on the dawnside magnetotail equatorial plane. In Figure 4c, the J-shaped TPA's source region extended from the duskside at  $X \sim -16 R_E$  to the dawnside at  $X \sim -90 R_E$ , over  $\sim 20 R_E$  in the dawn-dusk direction across midnight. Note that this projection of the J-shaped TPA using the T96 field line model might be different from the actual mapping, because the field line model does not take into account magnetotail deformation and the associated field line twisting due to the intense IMF-

$B_Y$  effect that is necessary for forming a J-shaped TPA (Nowada et al., 2020).

The projection of the auroral spiral (Figure 4b) also elongated tailward, and its scale was  $\sim 20 R_E$  and  $\sim 4 R_E$  in the X and Y directions in GSM, respectively, even though the spiral had the form of a spot in the ionosphere. This elliptic form is consistent with the discussions by Kaufmann et al. (1990) for quiet time magnetosphere and Lu et al. (2000) during a substorm. The auroral spiral had almost the same scale as that seen at different times on the same day (Nowada et al., 2023).

To discuss the detailed formation process of these auroral phenomena, we also performed global magnetohydrodynamic (MHD) computer simulations using the Block-Adaptive-Tree-Solar wind-Roe-Upwind-Scheme (BAT-S-RUS) code provided by the Community Coordinated Modeling Center (CCMC) at NASA Goddard Space Flight Center (GSFC). Figure 5 shows the distributions of the FACs at the magnetic equatorial plane of the magnetotail (Figures 5a–5c) and the nightside ionosphere (Figures 5d–5f) reproduced by the BAT-S-RUS MHD simulation. Each time label is almost the same as that in Figure 4.

In all Figures 5a–5c, the field-aligned current (FAC) sheet structures were clearly generated in the dawn sector (Figures 5a and 5b) and in the dawn to midnight sector (Figure 5c). The FAC sheets seen in Figures 5a and 5c correspond to the nightside TPA projections shown in Figures 4a and 4c. The FAC sheet profile of the J-shaped TPA in the magnetotail reproduced by the MHD simulation (Figure 5c) is totally different from that of the Polar observation (Figure 4c), because, in the Polar observation, each UVI pixel data were simply traced back along the T96 model field lines without considering the magnetotail twisting due to significant IMF- $B_Y$  effects. Taking a look at Figure 5f, however, the J-shaped TPA can be reproduced in the ionosphere with the simulation, and the dawn-dusk distributed FAC structure that extended tailward as shown in Figure 5c might agree with the actual J-shaped-TPA-associated FAC profile. According to a J-shaped TPA formation model derived by the magnetotail observation (Nowada et al., 2020; particularly see their Figure 7), as the J-shaped TPA is growing to the dayside polar cap, the corresponding TPA's FAC structure should extend toward the magnetotail, deformed by the IMF- $B_Y$ . Hence, the simulation result can explain well this J-shaped TPA formation model proposed by Nowada et al. (2020). On the contrast, the TPA that was growing straightforwardly to the dayside (Figure 5a) can be reproduced and explained well by the MHD simulation. The ion velocity vectors show large-scale clockwise vortices around these intense FAC sheets (blueish colored region) at  $X \sim -13.5$  to  $-45 R_E$  and  $Y \sim -2.0$  to  $-18.0 R_E$  (Figure 5a) or  $Y \sim 4.5$  to  $-18.0 R_E$  (Figure 5c), as indicated with dotted magenta

ovals. These large vortices should be the source of the FACs from the magnetotail to the ionosphere (downward FACs) associated with the TPAs.

Although the FAC sheet structure can also be seen in Figure 5b, Polar did not detect this structure in the corresponding region (Figure 4b). Furthermore, the tailward elongating structures that corresponded to the auroral spiral and spots as detected by Polar were reproduced neither by this MHD simulation nor by the improved REPPU code, as shown in Figures S1a and S1b in supporting information.

In Figures 5d and 5f, the FAC profiles corresponding to the oval-aligned and J-shaped TPAs, respectively, observed by the Polar UVI were seen in the nightside ionosphere. The auroral spiral, however, was not reproduced at the poleward edge of the nightside auroral oval (Figure 5e) because of absence of the tailward elongating structures on the magnetic equatorial plane. Hence, neither BAT-S-RUS nor improved REPPU global MHD simulation code can reproduce the auroral spiral in the nightside ionosphere.

### **3-5. Contemporaneous Appearances of TPA and Auroral Spiral: Observations and MHD Simulations**

In the previous sections, we showed that the TPA was reproduced by the two different types of global MHD code, while the auroral spiral (and auroral spots) at the poleward edge of the nightside auroral oval was (were) not. These results suggest that the global-scale TPA can be treated within an MHD framework, while the spiral cannot. To investigate this point in more detail, we discuss the case in which the global-scale TPA and the local-scale auroral spiral contemporaneously appeared. Figure 6 shows a Polar UVI snapshot (Figure 6a) and its projection onto the magnetic equatorial plane (Figure 6b) that were taken when the J-shaped TPA and the auroral spiral were concomitant at 21:08:40 UT. At this time, the auroral spiral was also detected by the all-sky camera installed at Longyearbyen (Nowada et al., 2023).

Interestingly, the magnetic equatorial projections of both auroras had tailward elongating structures: in the dawn sector in  $-80 < X_{\text{gsm}} < -11 R_E$  and  $-20 < Y_{\text{gsm}} < -3 R_E$  for the J-shaped TPA, and in the dusk side sector in  $-75 < X_{\text{gsm}} < -38 R_E$  and  $6 < Y_{\text{gsm}} < 9 R_E$  for the auroral spiral. The X range of the J-shaped TPA was  $\sim 32 R_E$ , longer than that of the spiral, and the Y scale of the J-shaped TPA was about 6 times larger than that of the spiral.

With the BAS-T-RUS code, we also tried to simulate the FAC structures in the magnetotail and

the auroral profiles in the ionosphere. Figure 7 shows the comparison of the Polar UVI observation with the BAT-S-RUS MHD simulation results. The magnetic equatorial map of the Polar UVI image is shown in Figure 7a, and Figures 7b and 7c show the distributions of FACs ( $J_{//}$  and  $J_{//z}$ , respectively) on the magnetic equatorial plane. Interestingly, neither the FAC profile in the source region of the J-shaped TPA (highlighted with magenta ovals) nor that of the auroral spiral (orange and green ovals) was reproduced by the global MHD simulation, although the intense  $J_{//}$  and weak  $J_{//z}$  were distributed at the J-shaped TPA source region in the dawn sector. The clear tailward-elongating FAC sheet structure associated with the oval-aligned TPA and J-shaped TPA, as seen in Figures 4a, 4c, 5a, 5c, 6 and 7a, was not observed in Figures 7b and 7c. For the spiral source, the profiles of  $J_{//}$  and  $J_{//z}$  could not be found.

To examine these FAC profiles in more detail, we zoomed in the FAC profiles at the auroral spiral, changing the color scale. Figure 8 shows the zoomed-in plots of the  $J_{//}$  (Figure 8a) and  $J_{//z}$  (Figure 8b) profiles at the source region of the auroral spiral identified with the Polar UVI observations. Both  $J_{//}$  and  $J_{//z}$  components did not show characteristic FAC structures at the spiral source region, although only very weak background current distributions in the out-of-plane sense can be found even though the color scale was changed. The flow velocities show no clear vortices or vortex-like structures that induce the FACs associated with the auroral spiral. These results suggest that the global MHD simulation may not reproduce the precise FAC profile associated with the auroral spiral in the magnetotail.

Similarly to the BAT-S-RUS simulation, the improved REPPU MHD simulation also did not reproduce and hence cannot explain in detail concomitance of the FAC sheet structure associated with the J-shaped TPA and the tailward elongating structure that corresponds to the auroral spiral (see Figures S1c and S1d).

### 3.6 Comparison of the Results from the Two Different Types of MHD Code

Figure 9 shows the comparison between the MHD reproductions of the nightside ionosphere during contemporaneous appearances of the J-shaped TPA and the auroral spiral, based on the BAT-S-RUS code (panel a) and the improved REPPU code (panels b and c). Both simulations reproduced well fundamental ionospheric FAC systems from the ionosphere (magnetosphere) to the magnetosphere (ionosphere) as indicated by blue (red). Neither the J-shaped TPA nor the auroral spiral at the poleward edge of the auroral oval was, however, reproduced, indicating that

the TPA treated within a global-scale MHD regime may be affected by the local-scale auroral spiral that was not reproduced by the MHD simulations as shown in Figures 5, 7 and 8. These results suggest that an auroral spiral and its formation process should be discussed within not an MHD regime but a kinetic framework.

### **3.7 Views from Ground-Based Observations: Spiral-Associated Geomagnetic Field Variations**

We investigated and argued the case of contemporaneous appearances of the J-shaped TPA and the auroral spiral, based on the Polar UVI observations and the global MHD simulations with the BAT-S-RUS and improved REPPU code. Besides, using equivalent ionospheric currents (EICs) derived from geomagnetic field variations from the IMAGE (International Monitor for Auroral Geomagnetic Effects) ground observatory network (Tanskanen, 2009), we can estimate a profile of the FACs associated with the spiral (and the TPA). Figure 10 shows the EIC vectors every 1min. from 21:05 UT to 21:10 UT. EICs were reconstructed by fitting spherical elementary currents to the measured magnetic field after decomposing the pure ionospheric current contribution and the telluric current component from the raw IMAGE geomagnetic field data. This EIC reconstruction technique was designed by Vanhamäki and Juusola (2020). The plotted EIC vectors roughly correspond to derivations of the ionospheric horizontal magnetic field components (local magnetic north-south and east-west components) by 90° clockwise. During the present time interval including the time when the spiral and the J-shaped TPA appeared contemporaneously (particularly, 21:08 UT), counter-clockwise rotations of the EIC vectors are seen at the spiral, shown with curved green arrows. These EIC profiles enable us to estimate that FACs were flowing upward from the ionosphere to the magnetotail associated with the spiral (as highlighted by bluish color). These FAC and EIC senses are consistent with that of the FACs in a local MHD simulation by Lysak and Song (1996) and a series of spirals (Davis and Hallinan, 1976; Partamies et al., 2001a). Because most part of the TPAs observed before, during, and after the spiral were lying over the Arctic Ocean, the magnetometers to measure the geomagnetic field deviations over the whole TPA were absent.

Figure 11 shows deviations of  $B_N$  component (local magnetic north-south direction) and its power spectrograms at three ground magnetometer observatories near the auroral spiral (indicated with the three magenta dots in the UVI plot) during the auroral spiral and contemporaneous appearances

of the TPA and the spiral from 19:59 UT to 21:23 UT. The  $B_N$  deviations were derived by subtracting the magnetic field DC component from the observed magnetic field, and the power spectra were calculated from the wavelet analysis (Torrence and Compo, 1998). The frequency band of Pc5 ultra-low-frequency (ULF: 1.67 mHz-6.67 mHz) waves is bracketed by green horizontal broken lines. The two times of interest of 20:16:32 UT (fine auroral spiral) and 21:08:40 UT (contemporaneous appearances of the J-shaped TPA and the auroral spiral) are indicated by sky blue and orange vertical broken lines, respectively. The plots of deviations of  $B_E$  (local magnetic east-west direction) and  $B_z$  (vertical up-down direction) and their power spectrograms during the same time interval as Figure 11 are shown in Figure S2 in supporting information.

Although the  $B_N$  component and the other two components show the perturbations (or waves) in the Pc5 ULF frequency range during the present interval, clear ULF waves were not always seen. Hence, we cannot conclude whether or not Pc5 ULF waves themselves play a role in auroral spiral formation, which would be the case in, for instance, auroral particle acceleration due to field line resonance (Rankin et al., 2005).

#### **4. Summary and Discussions**

The auroral spiral observed during the late stage of the substorm recovery phase on 10 January 1997 appeared after the oval-aligned TPA, followed by contemporaneous appearances of the nightside distorted TPA (J-shaped TPA) and the auroral spiral and then by only the J-shaped TPA. Nowada et al. (2023) focused on the auroral morphological changes after the substorm expansion phase, particularly auroral spiral formation, for the present event and clarified how the auroral spiral and its source in the magnetotail were formed. On the other hand, in this study, we tried to explain how a local-scale spiral can affect a global-scale TPA because these two auroral phenomena with different scales contemporaneously appeared.

To examine the FAC profiles in the magnetotail and ionospheric processes during concomitance of the J-shaped TPA and the spiral, we performed global MHD simulations using two different types of MHD code of BAT-S-RUS and improved REPPU. These simulations reproduced the global-scale TPA and the associated magnetotail FAC structure, but the local-scale auroral spiral and its concomitance with the TPA were not generated in the polar cap region and the magnetotail. An interesting point here is that the J-shaped TPA that should be treated within an MHD regime could not be reproduced by global MHD simulations, when it appeared together with the local-

scale auroral spiral. This result suggests that the formation process of the auroral spiral, which might not be discussed within an MHD regime, that is, can be related with some kinetic effect, could influence the MHD-scale TPA formation. Table 1 summarizes the temporal transitions of the auroral type, corresponding IMF-B<sub>Z</sub> conditions, and auroral reproductions by the global MHD simulations.

Depending on the substorm phases, the corresponding magnetotail dynamics, including the magnetic field and plasma variations, totally differ. Therefore, it might be natural that the formation process of the auroral spirals during the substorm expansion phase as addressed within an MHD regime (shear flow ballooning instability) and as examined by Keiling et al. (2009b) and Voronkov et al. (2000) does not apply to our auroral spiral during the late stage of a substorm recovery phase. If we consider that Huang et al. (2022) succeeded to reproduce the spiral by the Particle-In-Cell (PIC) simulation, it can be valid to conclude that the auroral spiral formation is more effective in a kinetic process than in an MHD effect, although their spiral formation region and main mechanism are totally different from ours.

The perturbations (rather than waves) in the ULF Pc5 band were also observed, so their role in auroral spiral formation should be considered in future works by performing again global MHD simulations with higher temporal and spatial resolutions, that is, simulations with the improved REPPU code with a high order number grid splitting. Furthermore, based on computer simulations using the PIC and hybrid-Vlasov (Vlasiator; Palmroth et al., 2018) code, we will examine whether or not the auroral spiral (and spots) at the poleward edge of the nightside auroral oval and its (their) source region(s) in the nightside magnetosphere can be reproduced from a kinetic point of view.

## **Acknowledgments**

M.N. enjoyed fruitful and constructive discussions with Qiu-Gang Zong, Alexander William Degeling, Timo Pitkänen, and Jong-Sun Park and was supported by a grant of the National Natural Science Foundation of China (NSFC 42074194). Y.M. was supported by basic research funding from Korea Astronomy and Space Science Institute (KASI2024185002). N.P. was supported by the Norwegian Research Council (NRC) under CoE contract 223252. Q.Q.S. was supported by NSFC 41731068, 41961130382, and 41974189. We thank George K. Parks for providing the Polar UVI data and Kan Liou for processing the data. We thank the institutes that maintain the IMAGE Magnetometer Array: Tromsø Geophysical Observatory of UiT, the Arctic University of Norway



(Norway), Finnish Meteorological Institute (Finland), Institute of Geophysics, Polish Academy of Sciences (Poland), GFZ German Research Centre for Geosciences (Germany), Geological Survey of Sweden (Sweden), Swedish Institute of Space Physics (Sweden), Sodankylä Geophysical Observatory of the University of Oulu (Finland), Polar Geophysical Institute (Russia), DTU Technical University of Denmark (Denmark), and Science Institute of the University of Iceland (Iceland).

### Data Accessibility

Polar ultraviolet imager (UVI) level-1 data can be accessed from [https://cdaweb.gsfc.nasa.gov/pub/data/polar/uvi/uvi\\_level1/](https://cdaweb.gsfc.nasa.gov/pub/data/polar/uvi/uvi_level1/). Data for calibrating the level-1 data and calculating the position of the UVI images can be accessed from <https://doi.org/10.6084/m9.figshare.5197084.v1> (Uritsky and POLAR UVI team, 2017). All IMAGE magnetometer numerical data used in Figure 10 can be downloaded from the IMAGE website ([https://space.fmi.fi/image/www/?page=user\\_defined](https://space.fmi.fi/image/www/?page=user_defined)). The numerical data from the magnetometers used in Figure 11 as well as the *SML* and *SMU* indices can be downloaded from the SuperMAG website (<https://supermag.jhuapl.edu/mag/>). The OMNI solar wind magnetic field and plasma data can be acquired from Coordinated Data Analysis Web ([https://cdaweb.gsfc.nasa.gov/pub/data/omni/omni\\_cdaweb/hro\\_1min/1997/](https://cdaweb.gsfc.nasa.gov/pub/data/omni/omni_cdaweb/hro_1min/1997/)), which is administrated by GSFC/NASA. The  $K_p$  index is provided by the Helmholtz Centre Potsdam - GFZ German Research Centre for Geosciences (<https://kp.gfz-potsdam.de/en/>). We also gratefully acknowledge the SuperMAG collaborators (<https://supermag.jhuapl.edu/info/?page=acknowledgement>) for using the *SML* and *SMU* indices. The BAT-S-RUS MHD simulation results can be referred to the three runs of Motoharu\_Nowada\_112620\_1 ([https://ccmc.gsfc.nasa.gov/results/viewrun.php?domain=GM&runnumber=Motoharu\\_Nowada\\_112620\\_1](https://ccmc.gsfc.nasa.gov/results/viewrun.php?domain=GM&runnumber=Motoharu_Nowada_112620_1)), Motoharu\_Nowada\_090923\_3 ([https://ccmc.gsfc.nasa.gov/results/viewrun.php?domain=GM&runnumber=Motoharu\\_Nowada\\_090923\\_3](https://ccmc.gsfc.nasa.gov/results/viewrun.php?domain=GM&runnumber=Motoharu_Nowada_090923_3)), and Motoharu\_Nowada\_090523\_1 ([https://ccmc.gsfc.nasa.gov/results/viewrun.php?domain=GM&runnumber=Motoharu\\_Nowada\\_090523\\_1](https://ccmc.gsfc.nasa.gov/results/viewrun.php?domain=GM&runnumber=Motoharu_Nowada_090523_1)) in the CCMC. All numerical data of the REPPU global MHD simulation results in this study are available in Nowada et al. (2024).

## References

- Angelopoulos, V., Cruce, P., Drozdov, A. et al. (2019). The Space Physics Environment Data Analysis System (SPEDAS). *Space Sci. Rev.*, 215, 9. <https://doi.org/10.1007/s11214-018-0576-4>.
- Baker, K. B., and Wing, S. (1989). A new magnetic coordinate system for conjugate studies at high latitudes. *J. Geophys. Res. -Space Physics-*, 94(A7), 9,139 – 9,143. <https://doi.org/10.1029/JA094iA07p09139>.
- Carter, J. A., Milan, S. E., Fear, R. C., Walach, M.-T., Harrison, Z. A., Paxton, L. J., and Hubert, B. (2017). Transpolar arcs observed simultaneously in both hemispheres. *J. Geophys. Res. -Space Physics-*, 122, 6,107 – 6,120. <https://doi.org/10.1002/2016JA023830>.
- Cowley, S. W. H. (1981). Magnetospheric asymmetries associated with the y-component of the IMF. *Planet. Space Sci.*, 29, 1, 79 – 96. [https://doi.org/10.1016/0032-0633\(81\)90141-0](https://doi.org/10.1016/0032-0633(81)90141-0).
- Cowley, S. W. H. (1994). Earth's plasma environment: magnetic reconnection and its effect on magnetospheric fields and flows. *Philosophical Transaction: Physical Sciences and Engineering*, 349, 1690, *The Solar-System: A Review of Results from Space Mission (Nov. 15)*, 237 – 247. <https://doi.org/10.1098/rsta.1994.0128>.
- Davis, T. N., and Hallinan, T. J. (1976). Auroral spirals, 1. Observations. *J. Geophys. Res.*, 81(22), 3,953 – 3,958. <https://doi.org/10.1029/JA081i022p03953>.
- Elphinstone, R. D., et al. (1995). The double oval UV auroral distribution: 1. Implications for the mapping of auroral arcs. *J. Geophys. Res. -Space Physics-*, 100(A7), 12,075 – 12,092. <https://doi.org/10.1029/95JA00326>.
- Fear, R. C., and Milan, S. E. (2012a). The IMF dependence of the local time of transpolar arcs: Implications for formation mechanism. *J. Geophys. Res. -Space Physics-*, 117(A03213). <https://doi.org/10.1029/2011JA017209>.
- Fear, R. C., and Milan, S. E. (2012b). Ionospheric flows relating to transpolar arc formation, *J. Geophys. Res. -Space Physics-*, 117(A09230). <https://doi.org/10.1029/2012JA017830>.
- Frank, L. A., J. D. Craven, J. L. Burch, and Winningham, J. D. (1982). Polar views of the Earth's aurora with Dynamics Explorer. *Geophys. Res. Lett.*, 9(9), 1,001 – 1,004. <https://doi.org/10.1029/GL009i009p01001>.
- Gjerloev, J. W. (2012). The SuperMAG data processing technique, *J. Geophys. Res. -Space Physics-*, 117, A09213, <https://doi.org/10.1029/2012JA017683>.

- Gosling, J. T., Thomsen, M. F., Bame, S. J., Elphic, R. C., and Russell, C. T. (1990). Plasma flow reversals at the dayside magnetopause and the origin of asymmetric polar cap convection. *J. Geophys. Res., -Space physics-*, 95(A6), 8,073 – 8,084. doi:10.1029/JA095iA06p08073.
- Hallinan, T. J., and Davis, T. N. (1970). Small-scale auroral arc distortions. *Planet. Space Sci.*, 18(12), 1,735 – 1,744. [https://doi.org/10.1016/0032-0633\(70\)90007-3](https://doi.org/10.1016/0032-0633(70)90007-3).
- Hallinan, T. J. (1976). Auroral spirals, 2. Theory. *J. Geophys. Res.*, 81(22), 3,959 – 3,965. <https://doi.org/10.1029/JA081i022p03959>.
- Kaufmann, R. L., Larson, D. J., and Lu, C. (1990). Mapping and distortions of auroral structures in the quiet magnetosphere. *J. Geophys. Res. -Space Physics-*, 95(A6), 7,973 – 7,994. <https://doi.org/10.1029/JA095iA06p07973>.
- Keiling, A., Angelopoulos, V., Runov, A., Weygand, J., Apatenkov, S. V., Mende, S., et al. (2009a). Substorm current wedge driven by plasma flow vortices: THEMIS observations. *J. Geophys. Res. -Space Physics-*, 114(A1), A00C22. <https://doi.org/10.1029/2009JA014114>.
- Keiling, A., Angelopoulos, V., Weygand, J. M., Amm, O., Spanswick, E., Donovan, E., Mende, S., McFadden, J., Larson, D., Glassmeier, K.-H., and Auster, H. U. (2009b). THEMIS ground-space observations during the development of auroral spirals. *Ann. Geophys.*, 27, 11, 4,317 – 4,332. <https://doi.org/10.5194/angeo-27-4317-2009>.
- Kullen, A., Brittnacher, M., Cumnock, J., and Blomberg, L. (2002). Solar wind dependence of the occurrence and motion of polar auroral arcs: A statistical study. *J. Geophys. Res. -Space Physics-*, 107(A11), 1362. <https://doi.org/10.1029/2002JA009245>.
- Kullen, A., and Janhunen, P. (2004). Relation of polar auroral arcs to magnetotail twisting and IMF rotation: a systematic MHD simulation study. *Ann. Geophys.*, 22, 3, 951 – 970. <https://doi.org/10.5194/angeo-22-951-2004>.
- Kullen, A., Fear, R. C., Milan, S. E., Carter, J. A., and Karlsson T. (2015). The statistical difference between bending arcs and regular polar arcs. *J. Geophys. Res. -Space Physics-*, 120, 10,443 – 10,465. <https://doi.org/10.1002/2015JA021298>.
- Lu, G., Brittnacher, M., Parks, G., and Lummerzheim, D. (2000). On the magnetospheric source regions of substorm-related field-aligned currents and auroral precipitation. *J. Geophys. Res. -Space Physics-*, 105(A8), 18,483 – 18,493. <https://doi.org/10.1029/1999JA000365>.
- Lysak, R. L., and Song, Y. (1996). Coupling of Kelvin-Helmholtz and current sheet instabilities to the ionosphere: A dynamic theory of auroral spirals. *J. Geophys. Res. -Space Physics-*, 101(A7),

15,411 – 15,422. <https://doi.org/10.1029/96JA00521>.

- Milan, S. E., Hubert, B., and Grocott, A. (2005). Formation and motion of a transpolar arc in response to dayside and nightside reconnection. *J. Geophys. Res. -Space Physics-*, 110(A01212). <https://doi.org/10.1029/2004JA010835>.
- Huang, K., Liu, Y.-H., Lu, Q., Hu, Z., Lynch, K. A., Hesse, M., et al. (2022), Auroral spiral structure formation through magnetic reconnection in the auroral acceleration region, *Geophys. Res. Lett.*, 49, <https://doi.org/10.1029/2022GL100466>.
- Murphree, J. S., and Cogger, L. L. (1981). Observed connections between apparent polar-cap features and the instantaneous diffuse auroral oval. *Planet. Space Sci.*, 29(11), 1,143 – 1,149. [https://doi.org/10.1016/0032-0633\(81\)90120-3](https://doi.org/10.1016/0032-0633(81)90120-3).
- Nakamizo, A., Tanaka, T., Kubo, Y., Kamei, S., Shimazu, H., and Shinagawa, H. (2009). Development of the 3-D MHD model of the solar corona-solar wind combining system. *J. Geophys. Res. -Space Physics-*, 114, A07109. <https://doi.org/10.1029/2008JA013844>.
- Newell, P. T., and Gjerloev, J. W. (2011). Evaluation of SuperMAG auroral electrojet indices as indicators of substorms and auroral power. *J. Geophys. Res. -Space Physics-*, 116, A12211, <https://doi.org/10.1029/2011JA016779>.
- Nowada, M., Fear, R. C., Grocott, A., Shi, Q. -Q., Yang, J., Zong, Q. -G., et al. (2018). Subsidence of ionospheric flows triggered by magnetotail magnetic reconnection during transpolar arc brightening. *J. Geophys. Res. -Space Physics-*, 123, 3,398 – 3,420. <https://doi.org/10.1029/2017JA024701>.
- Nowada, M., Zong, Q. -G., Hubert, B., Shi, Q. -Q., Wang, Y.-F., Yang, J., et al. (2020). North-south asymmetric nightside distorted transpolar arcs within a framework of deformed magnetosphere-ionosphere coupling: IMF-By dependence, ionospheric currents, and magnetotail reconnection. *J. Geophys. Res. -Space Physics-*, 125, 2020JA027991. <https://doi.org/10.1029/2020JA027991>.
- Nowada, M., Miyashita, Y., Partamies, N., Degeling, A. W., and Shi, Q. -Q. (2023). Auroral morphological changes to the formation of auroral spiral during the late substorm recovery phase: Polar UVI and ground all-sky camera observations. *J. Geophys. Res. -Space Physics-*, 128, e2023JA031400. <https://doi.org/10.1029/2023JA031400>.
- Nowada, M., Miyashita, Y., Nakamizo, A., Partamies, N., and Shi, Q. -Q. (2024). Numerical data of the REPPU global MHD simulation results (1<sup>st</sup> version published on 6<sup>th</sup> September, 2024)

- [Dataset]. Science Data Bank. <https://www.scidb.cn/en/anonymous/RIZGN3p1>.
- Palmroth, M., Ganse, U., Pfau-Kempf, Y., Battarbee, M., Turc, L., Brito, T., Grandin, M., Hoilijoki, S., Sandroos, A., and von Alfthan, S. (2018). Vlasov methods in space physics and astrophysics. *Living Rev. Comput. Astrophys.*, 4(1). <https://doi.org/10.1007/s41115-018-0003-2>.
- Parks, G., Brittnacher, M., Chen, L. J., Elsen, R., McCarthy, M., Germany, G., and Spann, J. (1997). Does the UVI on Polar detect cosmic snowballs? *Geophys. Res. Lett.*, 24(24), 3,109 – 3,112. <https://doi.org/10.1029/97GL03005>.
- Partamies, N., Kauristie, K., Pulkkinen, T. I., and Brittnacher, M. (2001a). Statistical study of auroral spirals. *J. Geophys. Res. -Space Physics-*, 106(A8), 15,415 – 15,428. <https://doi.org/10.1029/2000JA900172>.
- Partamies, N., Freeman, M. P., and Kauristie, K. (2001b). On the winding of auroral spirals: Interhemispheric observations and Hallinan's theory revisited. *J. Geophys. Res. -Space Physics-*, 106(A12), 28,913 – 28,924. <https://doi.org/10.1029/2001JA900093>.
- Perreault, P., and Akasofu, S. -I. (1978). Study of geomagnetic storms. *Geophys. J. R., Astron. Soc.*, 54, 3, 547 – 573. <https://doi.org/10.1111/j.1365-246X.1978.tb05494.x>.
- Rankin, R., K. Kabin, J. Y. Lu, I. R. Mann, R. Marchand, I. J. Rae, V. T. Tikhonchuk, and E. F. Donovan (2005). Magnetospheric field-line resonances: Ground-based observations and modeling. *J. Geophys. Res. -Space Physics-*, 110, A10S09. <https://doi.org/10.1029/2004JA010919>.
- Shue, J. -H., Song, P., Russell, C. T., Steinberg, J. T., Chao, J. K., Zastenker, G., Vaisberg, O. L., Kokubun, S., Singer, H. J., Detman, T. R., and Kawano, H. (1998), Magnetopause location under extreme solar wind conditions, *J. Geophys. Res. -Space Physics-*, 103(A8), 17691 – 17700, <https://doi.org/10.1029/98JA01103>.
- Tanaka, T. (1994). Finite volume TVD scheme on an unstructured grid system for three-dimensional MHD simulation of inhomogeneous systems including strong background potential fields. *J. Comput. Phys.*, 111, 2, 381 – 389. <https://doi.org/10.1006/jcph.1994.1071>.
- Tanaka, T., Obara, T., and Kunitake, M. (2004). Formation of the theta aurora by a transient convection during northward interplanetary magnetic field. *J. Geophys. Res., -Space Physics-*, 109, A09201. <https://doi.org/10.1029/2003JA010271>.
- Tanskanen, E. I. (2009). A comprehensive high-throughput analysis of substorms observed by IMAGE magnetometer network: Years 1993-2003 examined. *J. Geophys. Res. -Space Physics-*,

- 114, A05204, *J. Geophys. Res.*, 114, A05204. <https://doi.org/10.1029/2008JA013682>.
- Torr, M. R., Torr, D. G., Zukic, M., Johnson, R. B., Ajello, J., Banks, P., Clark, K., Cole, K., Keffer, C., Parks, G., Tsurutani, B., and Spann, J. (1995). A far ultraviolet imager for the International Solar-Terrestrial Physics Mission. *Space Sci. Rev.*, 71 (1-4), 329 – 383. <https://doi.org/10.1007/BF00751335>.
- Torrence, C., and Compo, G. P. (1998). A practical guide to wavelet analysis, *Bull. Am. Meteorol. Soc.*, 79, 1, 61 – 78, [https://doi.org/10.1175/1520-0477\(1998\)079<0061:APGTWA>2.0.CO;2](https://doi.org/10.1175/1520-0477(1998)079<0061:APGTWA>2.0.CO;2).
- Tsyganenko, N. A., and Fairfield, D. H. (2004). Global shape of the magnetotail current sheet as derived from Geotail and Polar data. *J. Geophys. Res. -Space Physics-*, 109(A03218). <https://doi.org/10.1029/2003JA010062>.
- Tsyganenko, N. A., and Sitnov, M. I. (2005). Modeling the dynamics of the inner magnetosphere during strong geomagnetic storms. *J. Geophys. Res. -Space physics-*, 110(A3), A03208. <https://doi.org/10.1029/2004JA010798>.
- Tsyganenko, N. A., and Stern, D. P. (1996), Modeling the global magnetic field of the large-scale Birkeland current systems. *J. Geophys. Res. -Space Physics-*, 101(A12), 27187 – 27198, <https://doi.org/10.1029/96JA02735>.
- Tsyganenko, N. A., Andreeva, V. A., and Gordeev, E. I. (2015). Internally and externally induced deformations of the magnetospheric equatorial current as inferred from spacecraft data. *Ann. Geophys.*, 33, 1, 1 – 11. <https://doi.org/10.5194/angeo-33-1-2015>.
- Uritsky, V., and POLAR UVI team (2017). POLAR UVI calibration toolkit [Dataset]. Figshare. <https://doi.org/10.6084/M9.FIGSHARE.5197084.V1>.
- Vanhamäki, H. and Juusola, L. (2020). Introduction to spherical elementary current systems, *Ionospheric Multi-Spacecraft Analysis Tools*, edited by: Dunlop, M. and Lühr, H., ISSI Scientific Report Series, 5 – 33, Vol. 17, Springer, Cham., [https://doi.org/10.1007/978-3-030-26732-2\\_2](https://doi.org/10.1007/978-3-030-26732-2_2).
- Voronkov, I., Donovan, E. F., Jackel, B. J., and Samson, J. C. (2000). Large-scale vortex dynamics in the evening and midnight auroral zone: Observations and simulations. *J. Geophys. Res.*, -Space Physics-, 105(A8), 18505–18518. <https://doi.org/10.1029/1999JA000442>.
- Watanabe, M., Sakito, S., Tanaka, T., Shinagawa, H., and Murata, K. T. (2014). Global MHD modeling of ionospheric convection and field-aligned currents associated with IMF By triggered theta auroras. *J. Geophys. Res.*, -Space Physics-, 119, 6,145 – 6,166. <https://doi.org/10.1002/2013JA019480>.

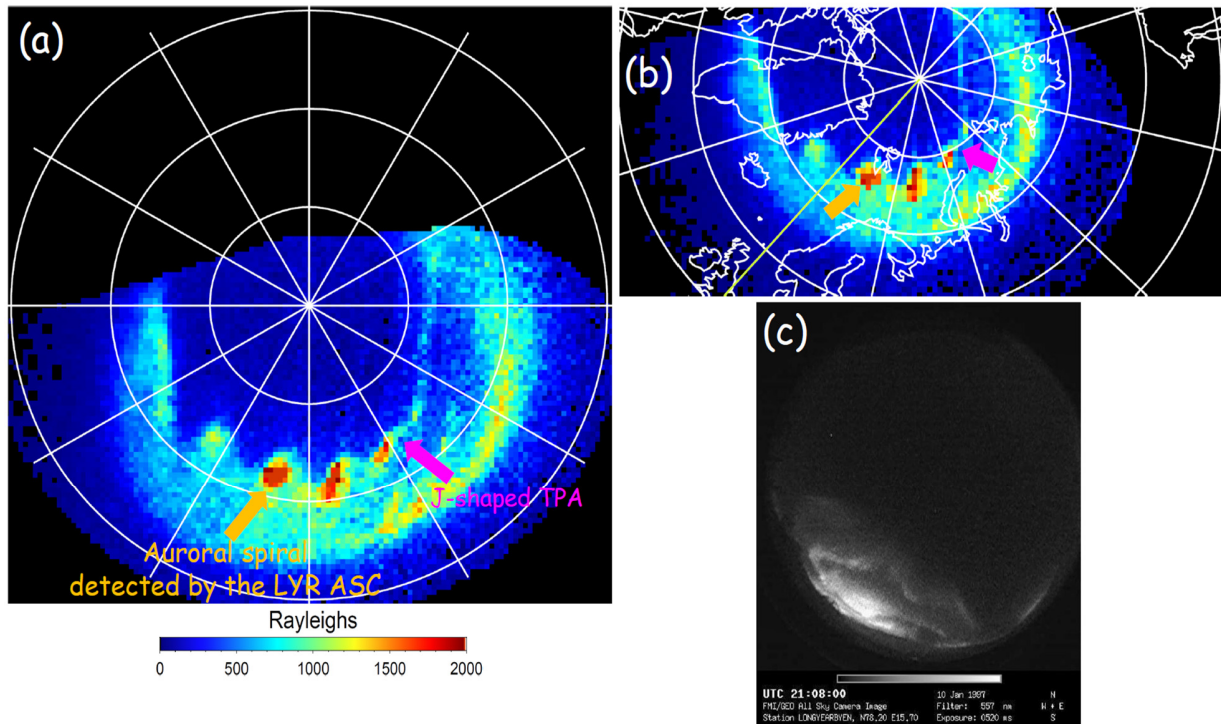


**Figure 1.** Fine snapshots of contemporaneous appearances of the auroral spiral (pointed out by thick orange arrows) and the nightside distorted transpolar arc (J-shaped TPA, indicated with thick magenta arrows) observed by Polar ultraviolet imager (UVI) and Longyearbyen all-sky camera (ASC) are shown. Panels a and b are Lyman-Birge-Hopfield short (LBHS) emission images with an integration time of 36 s in altitude adjusted corrected geomagnetic (AACGM; Baker and Wing, 1989) and geographic coordinate systems, respectively, at 21:08:40 UT on 10 January 1997. Panel a is oriented such that the bottom, right, top, and left correspond to midnight (0 h magnetic local time; MLT), dawn (6 h MLT), noon (12 h MLT), and dusk (18 h MLT), respectively. The white circles are drawn every  $10^\circ$  from  $60^\circ$  to  $80^\circ$  magnetic latitude (MLat) for panel a and from  $50^\circ$  to  $80^\circ$  geographic latitude for panel b. The white straight lines are drawn every 2 h in MLT. The color code is assigned according to the auroral brightness in units of Rayleigh. Panel c shows an image of the auroral spiral taken from the ASC installed at Longyearbyen for the nearest observational time of panels a and b.

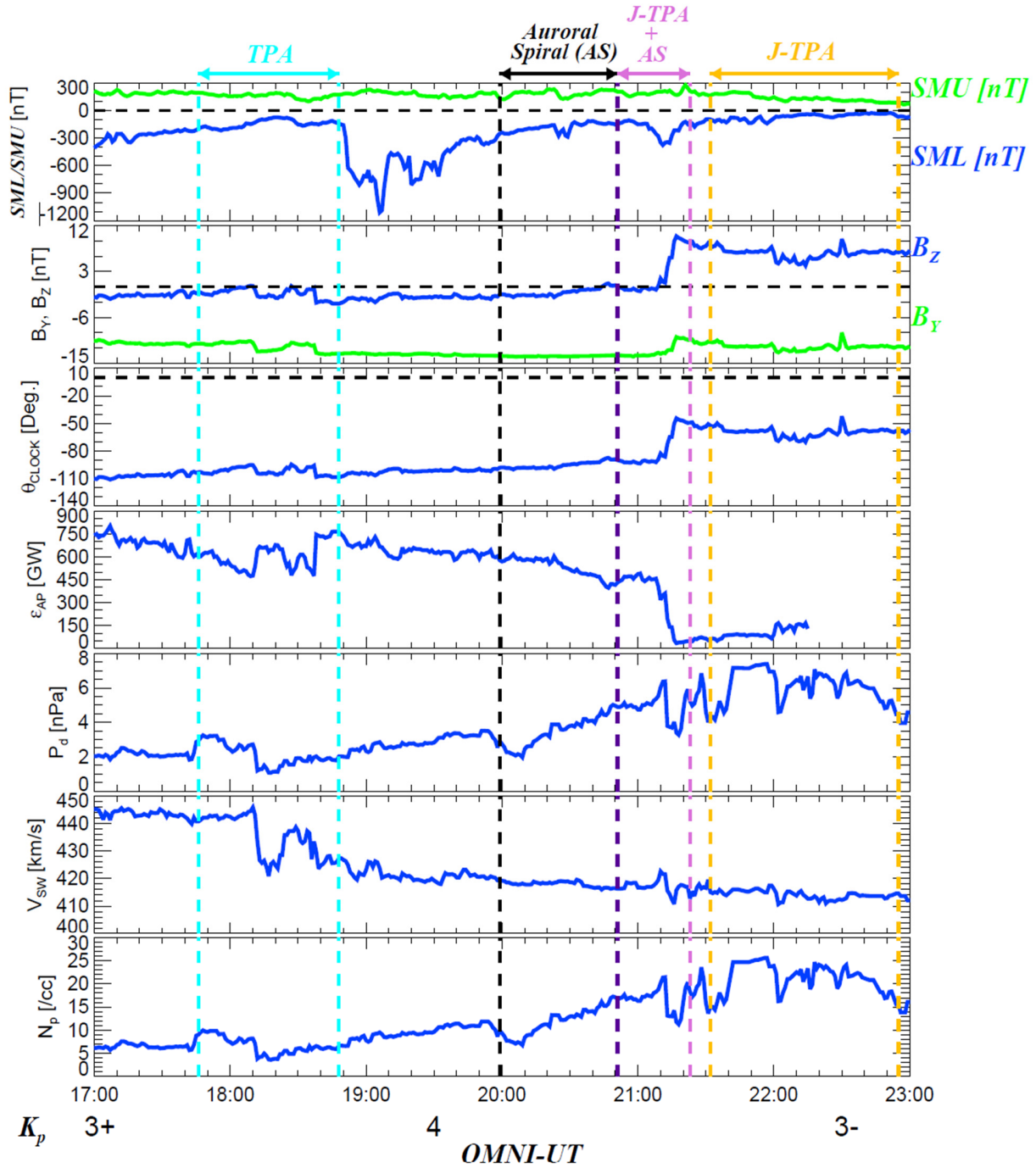


**Figure 2.** Plots of solar wind parameters and geomagnetic activity indices during the 6 h interval from 17:00 UT to 23:00 UT on 10 January 1997 are shown. From top to bottom: the  $SMU$  and  $SML$  indices which were derived, based on the high-latitude geomagnetic field data obtained from the SuperMAG geomagnetic observatory network (Newell and Gjerloev, 2011; Gjerloev, 2012); the IMF- $B_y$  and  $-B_z$  components; the IMF clock angle ( $\arctan(\text{IMF-}B_y/\text{IMF-}B_z)$ ); the Akasofu-



Pelleaut parameter ( $\epsilon_{AP}$ ) computed with  $V_{SW}B_t^2\sin^4(\theta_{CLOCK}/2)(4\pi L_0^2/\mu_0)$ , where  $V_{SW}$  is the solar wind velocity,  $B_t$  is the magnetic field intensity as calculated by  $\sqrt{IMF-B_X^2 + IMF-B_Y^2 + IMF-B_Z^2}$ , and  $L_0 = 7.0 R_E$ ; the solar wind dynamic pressure ( $P_d$ ); solar wind speed ( $V_{SW}$ ), and proton number density ( $N_P$ ). The  $K_p$  index is indicated at the bottom of the figure. The intervals of oval-aligned transpolar arc (TPA), auroral spiral, contemporaneous appearances of the J-shaped TPA and the auroral spiral, and the J-shaped TPA are bracketed with cyan, black, violet, and orange broken vertical lines, respectively.

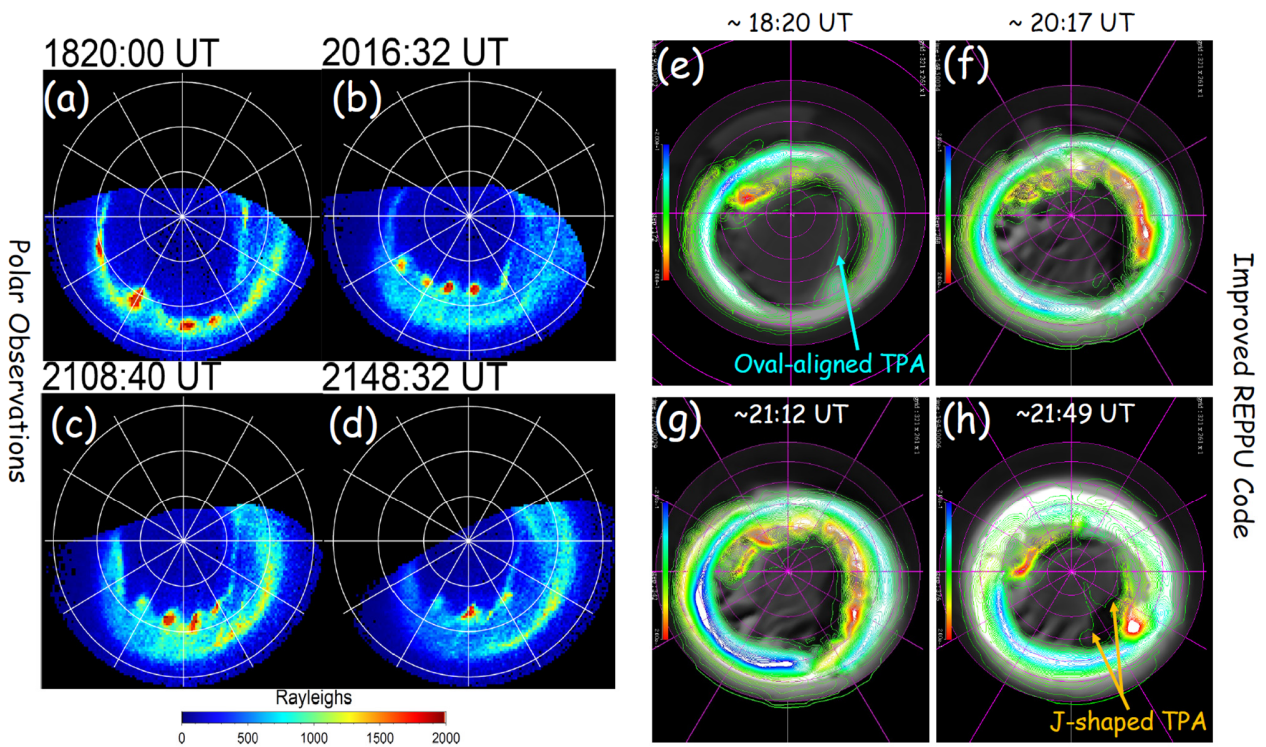


**Figure 3.** Representative snapshots of LBHL 36 s images of the four types of aurora and the corresponding snapshots of aurora-associated field-aligned current (FAC) density reproduced by a global MHD simulation using the improved REProduce Plasma Universe (REPPU) code are shown. The imager data plots of (a) oval-aligned TPA, (b) auroral spiral, (c) contemporaneous appearances of the TPA and the auroral spiral, and (d) J-shaped TPA are displayed. The color code is assigned according to the logarithm of auroral brightness in units of Rayleigh. The white circles are drawn every  $10^\circ$  from  $60^\circ$  to  $80^\circ$  magnetic latitude (MLat), and the white straight lines are drawn every 2 h in MLT. The color contours in panels e to h show the intensity of ionospheric conductance associated with auroras (a proxy of the FAC intensity), which is determined by magnetotail conditions. The reddish (bluish) color indicates the FACs toward (away from) the ionosphere. The magenta circles are drawn every  $5^\circ$  from  $65^\circ$  to  $90^\circ$  MLat, and the magenta straight lines are drawn every 2 h in MLT.

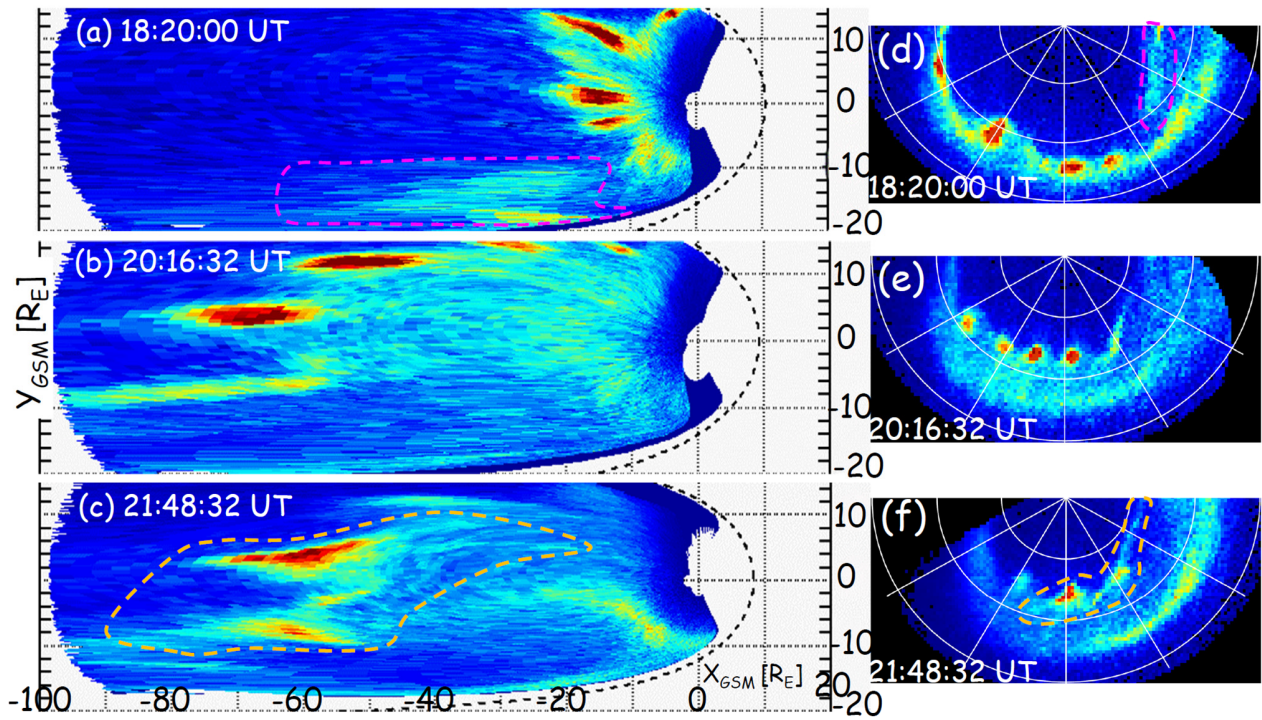


**Figure 4:** Magnetotail magnetic equatorial projections of Polar UVI auroral pixel data (panels a-c) and the original Polar UVI nightside ionospheric snapshots (panels d-f) for the oval-aligned TPA at 18:20:00 UT (panels a and d), the auroral spiral at 20:16:32 UT (panels b and e), and the J-shaped TPA at 21:48:32 UT (panels c and f) are shown. The format of panels d-f is the same as those of Figures 1a and 3a-3d, except that only the nightside in 18 to 6 h MLT is shown. The color code range is the same as that shown in Figure 3. Each UVI pixel is traced to the magnetic equatorial plane, based on the Tsyganenko 96 geomagnetic field model (Tsyganenko and Stern, 1996), using the calculation routines implemented in the Space Physics Environment Data Analysis Software (SPEDAS) 4.1 package (Angelopoulos et al., 2019). Magenta and orange broken ovals highlight the oval-aligned and J-shaped TPAs detected by Polar. The dashed black curves in panels a-c indicate the model magnetopause locations derived from Shue et al. (1998).

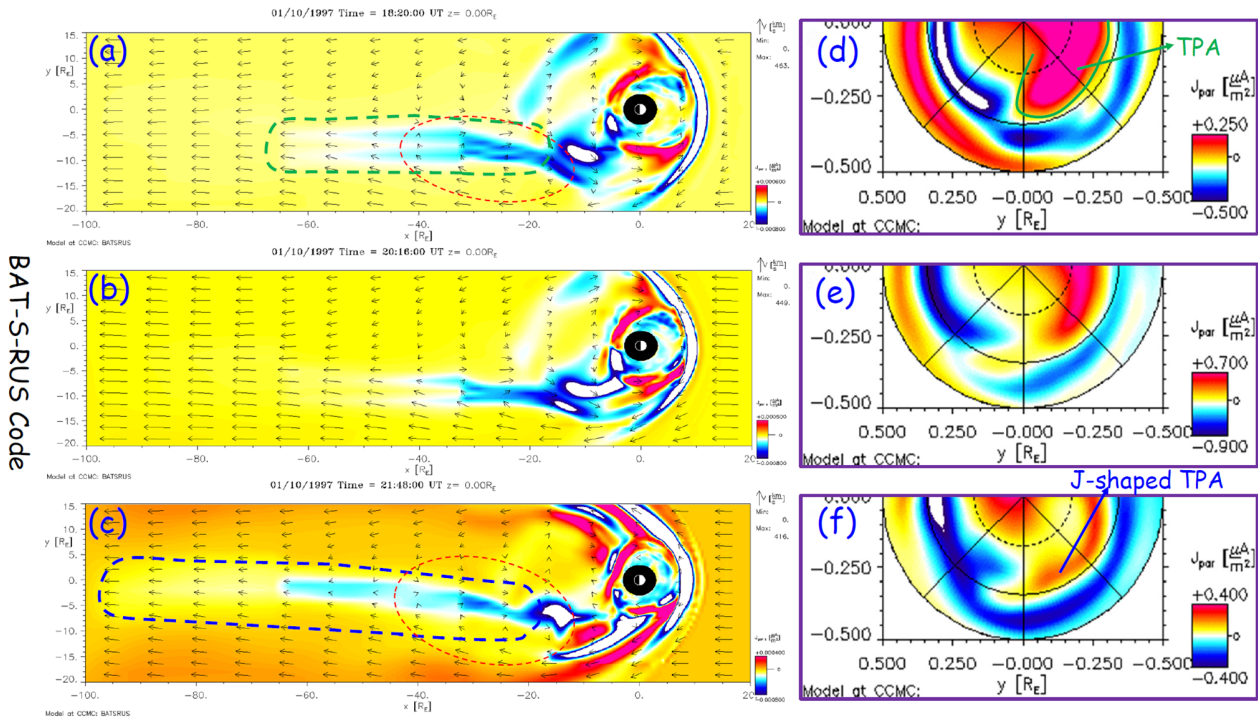


**Figure 5:** The density of field-aligned current (FAC) on the magnetic equatorial plane over the ranges of  $X = 20$  to  $-100 R_E$  and  $Y = 15$  to  $-20 R_E$  (panels a-c) and in the nightside ionosphere (panels d-f) in the oval-aligned TPA, the auroral spiral, and the J-shaped TPA cases are shown. These FAC structures are reproduced by the Block Adaptive Tree-Solar wind-Roe Upwind Scheme (BAT-S-RUS) code provided by the Community Coordinated Modeling Center (CCMC). In panels a to c, the color code is assigned according to the  $Z$  component (vertically up-down component to the  $X$ - $Y$  plane) of the FAC structures ( $J_{//z}$ ) on the magnetic equatorial plane in units of  $\mu A/m^2$ , and the ionospheric FACs ( $J_{//}$ ) are shown in panels d-f. The vectors in panels a-c indicate the plasma flow velocity ( $V_{XY}$ ) projected onto the magnetic equatorial plane in units of km/s.

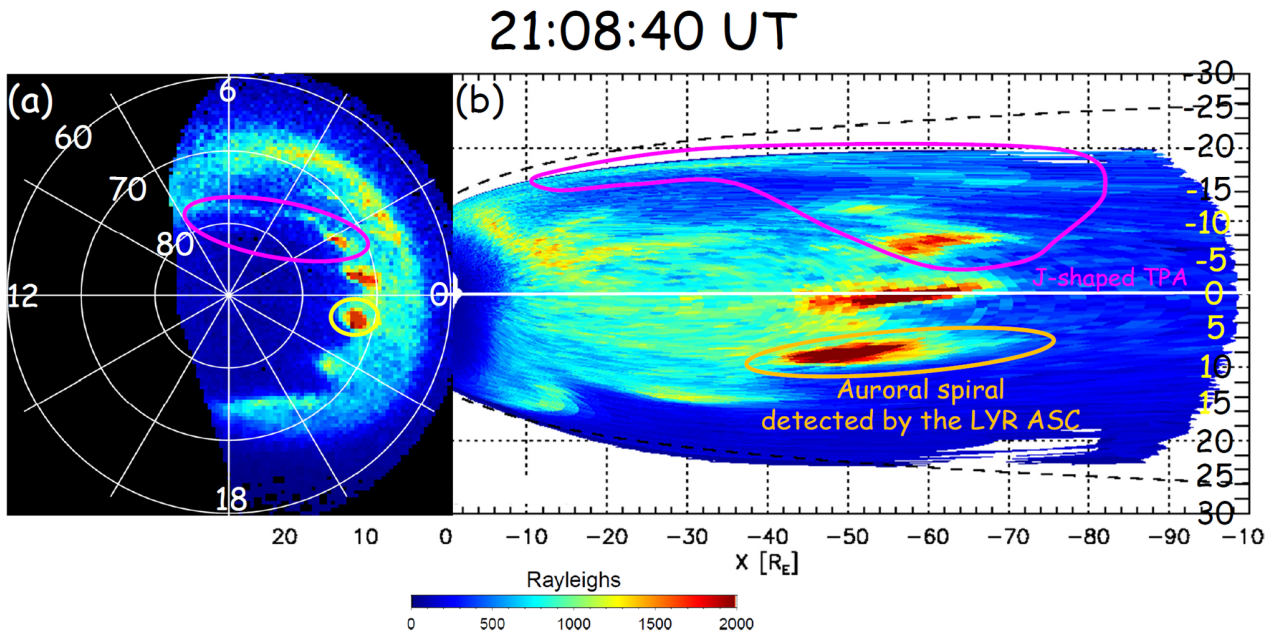


**Figure 6.** Polar UVI snapshot (panel a) and its magnetic equatorial projection (panel b) for contemporaneous appearances of the J-shaped TPA and the auroral spiral at 21:08:40 UT are shown. The format of the Polar UVI plot is the same as those of Figures 1a and 3a-3d, but the bottom, left, top, and right correspond to dusk (18 h in MLT), noon (12 h in MLT), dawn (6 h in MLT), and midnight (0 h in MLT), respectively. Yellow (orange) and magenta ovals indicate the auroral spiral detected by the Polar UVI and the ASC at Longyearbyen, and the J-shaped TPA by Polar, respectively. The color code shows the auroral brightness in units of Rayleigh. The dashed black curve indicates the model magnetopause location derived from Shue et al. (1998).

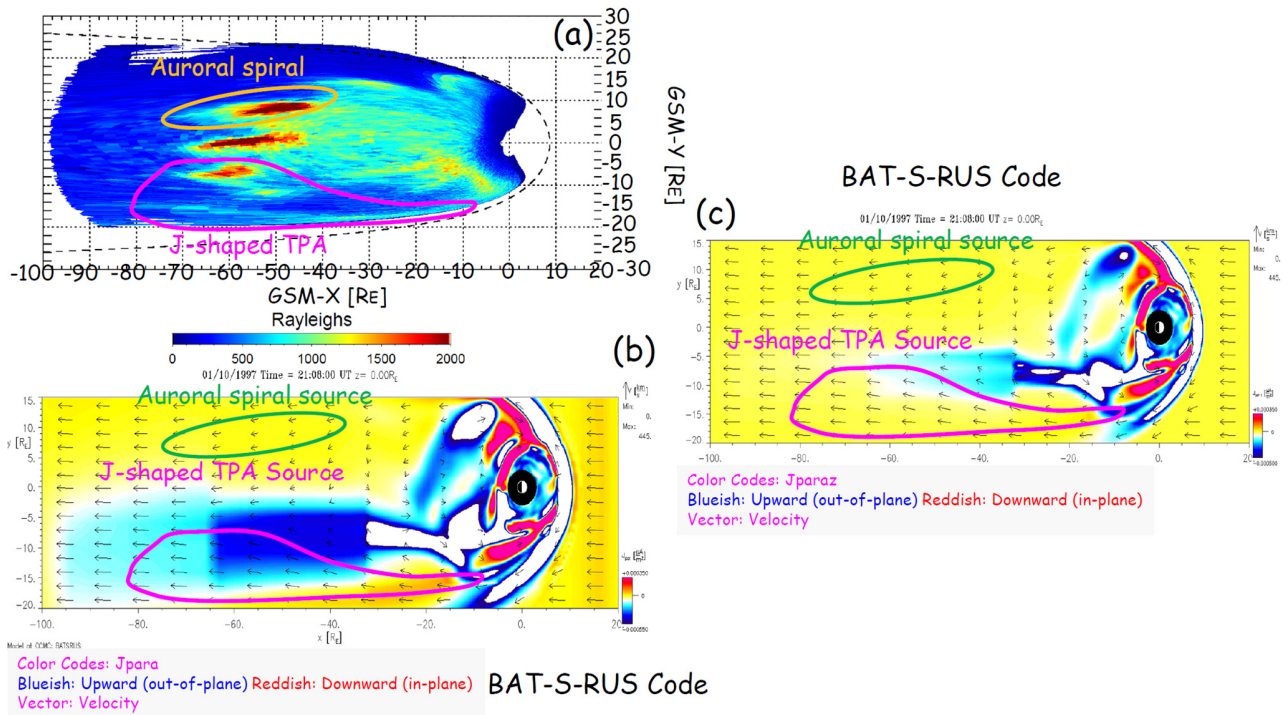


**Figure 7.** Three panels show the Polar UVI magnetic equatorial projection of the contemporaneous appearances of the J-shaped TPA and the auroral spiral at 21:08:40 UT (panel a), and the corresponding BAT-S-RUS global MHD simulation results on the equatorial plane over the ranges of  $X = 10$  to  $-100 R_E$  and  $Y = 15$  to  $-20 R_E$  (panels b and c). In panels b and c, the color code is assigned according to the FAC ( $J_{||}$ ) and the Z component of the FAC ( $J_{||z}$ ), respectively, in units of  $\mu A/m^2$ . The vectors indicate the plasma flow velocity ( $V_{xy}$ ) on the magnetic equatorial plane in units of km/s.

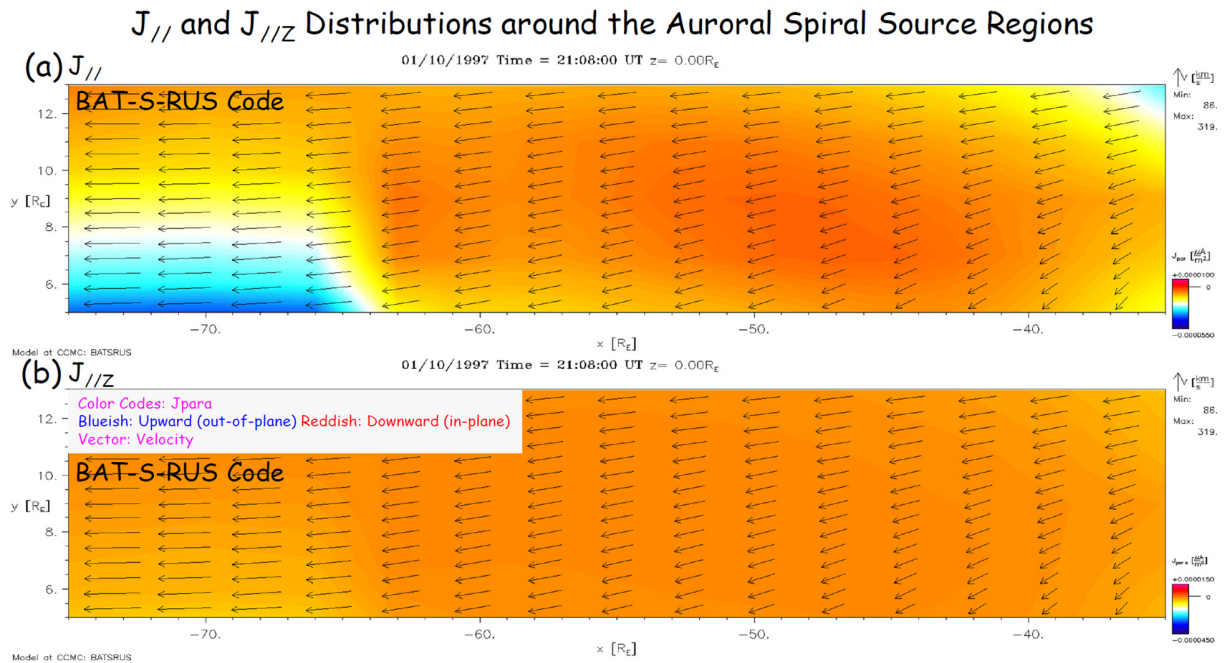


**Figure 8:** Zoom-in plots of the FAC ( $J_{//}$ ) (panel a) and the FAC Z-component ( $J_{//z}$ , panel b) at the auroral spiral source region at 21:08 UT are shown. The source region is determined by the Polar UVI observations, and these FAC distributions were reproduced by BAT-S-RUS global MHD simulations. The figure format is the same as those of Figures 5 and 7.

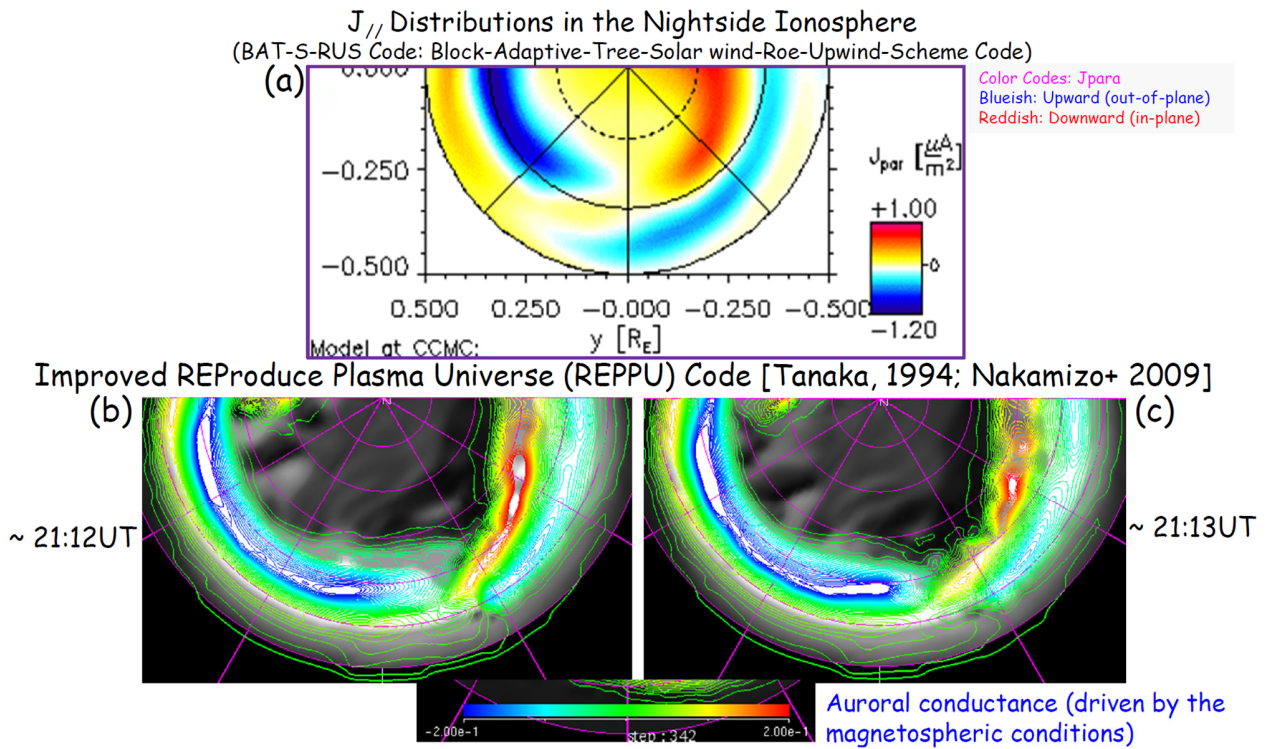


**Figure 9:** Comparison of the FACs reproduced by BAT-S-RUS (panel a) with the auroral conductance dependent on the magnetospheric conditions (a proxy of FACs) obtained from the improved REPPU code (panels b and c) around the times when the J-shaped TPA and auroral spiral were contemporaneously observed is shown.



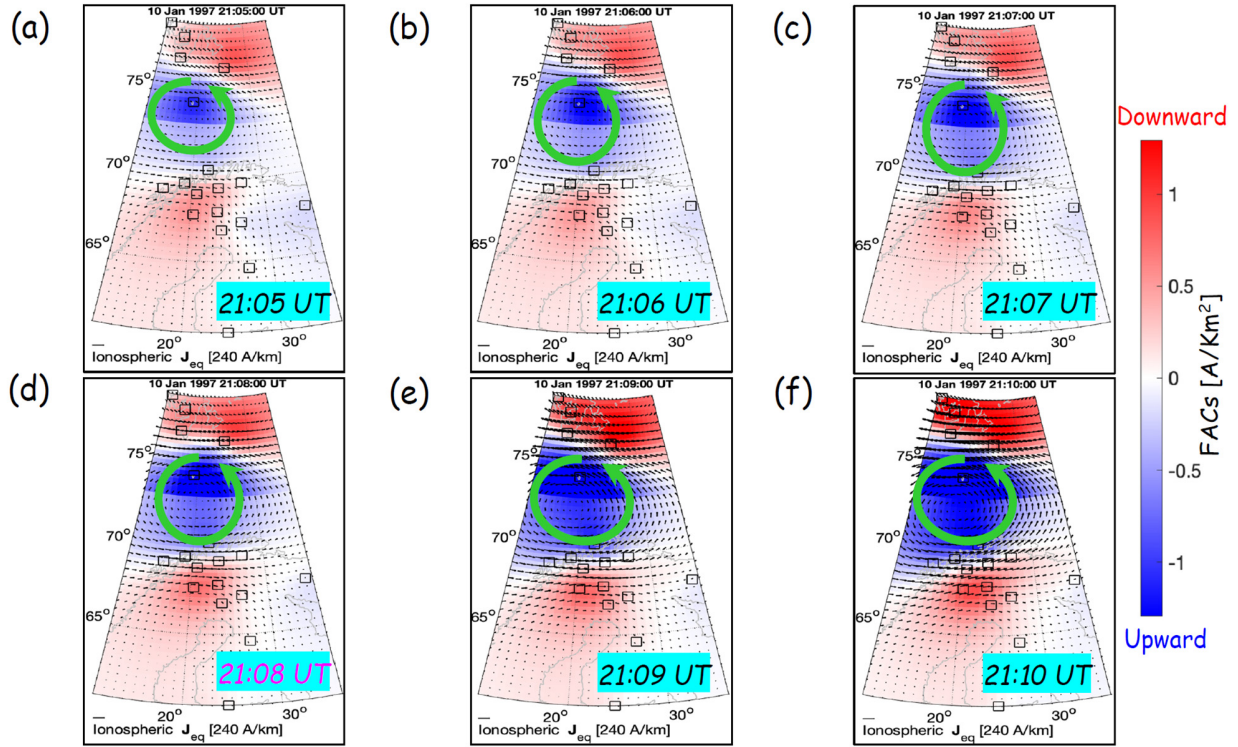


**Figure 10:** Counter-clockwise rotational vortex-like equivalent ionospheric electric current (EIC) structures, shown with curved green arrows, derived from the observations of the IMAGE ground observatory network (Tanskanen, 2009) near the auroral spiral region from 21:05 UT to 21:10 UT are shown with 1 min time step. These EIC vectors (black vectors) are derived by extracting the pure ionospheric current contribution by removing the telluric components from the measured geomagnetic field data, based on the technique proposed by Vanhamäki and Juusola (2020). The color code is assigned according to the FAC intensity (in unit of  $A/km^2$ ) and orientation estimated by the EIC vectors.

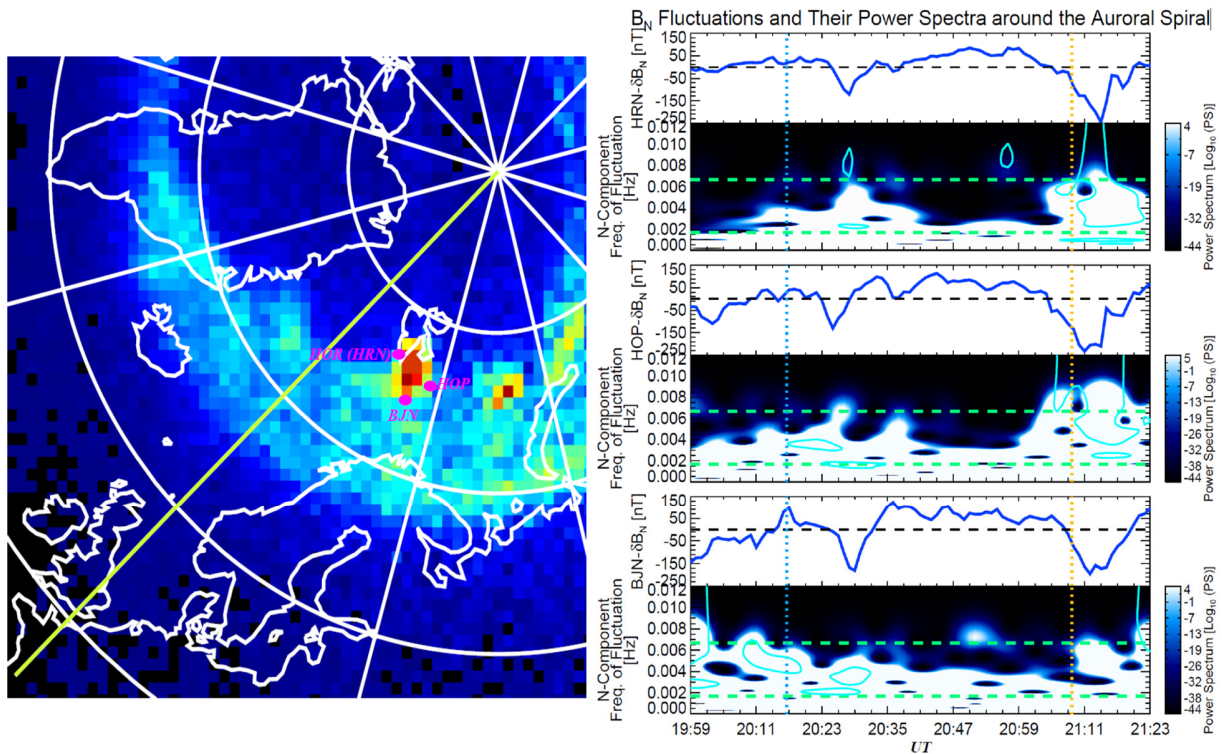


**Figure 11:** Map that shows the locations of three ground magnetometer stations relative to the auroral spiral on and near Svalbard is shown in the left panel. Deviations of the N component magnetic field ( $B_N$ , local magnetic north-south component) and their power spectrograms at HRN(HOR), HOP, and BUN stations during the auroral spiral intervals on and near the Svalbard Island from 19:59 UT to 21:23 UT are shown in the right panels. The power spectra of the  $B_N$  deviations are calculated, based on the wavelet analysis using the Morlet function (see Torrence and Compo, 1998 for details). In the power spectrograms, the confidence level higher than 93% for the wave power intensity is surrounded by cyan solid ovals. The frequency range of the Pc5 waves (1.67 - 6.67 mHz) is bracketed by two horizontal green broken lines. The two representative times of 20:16:32 UT (fine auroral spiral) and 21:08:40 UT (contemporaneous appearances of the J-shaped TPA and the auroral spiral) are indicated by sky blue and orange vertical broken lines, respectively.

**Table 1.** Transition of auroral shapes, IMF- $B_z$  conditions, the results of whether or not the observed auroras were reproduced by global MHD simulations, and the duration of the auroras seen during about 5 h interval from 17:46 UT to 22:55 UT are summarized, based on the Polar UVI observations.

	Auroral Type	IMF- $B_z$ Conditions	Reproduced by the MHD Simulations?	Time Interval (UT)	
				Duration (min.)	
(a)	Oval-aligned TPA	Weakly Southward	Yes	17:46 – 18:48	
				62	
(b)	Auroral Spiral	Weakly Southward with Transiently Northward	No	19:59 – 20:51	
				52	
(c)	J-shaped TPA + Auroral Spiral	Turning from Weakly Southward to Northward	TPA: No Auroral Spiral: No	20:51 – 21:23	
				32	
(d)	J-shaped TPA	Northward	Yes	21:32 – 22:55	
				83	

**Contemporaneous Appearances of Local-Scale Auroral Spirals and Global-Scale Transpolar Arc: Changes of Auroras and Field-Aligned Current Profiles Before a Substorm and After Its Recovery Phase**

Motoharu Nowada<sup>1\*</sup>, Yukinaga Miyashita<sup>2,3</sup>, Aoi Nakamizo<sup>4</sup>,  
Noora Partamies<sup>5</sup>, and Quan-Qi Shi<sup>1</sup>

- 1: Shandong Key Laboratory of Optical Astronomy and Solar-Terrestrial Environment, School of Space Science and Physics, Institute of Space Sciences, Shandong University, Weihai, Shandong, People's Republic of China.
- 2: Korea Astronomy and Space Science Institute, Daejeon, South Korea.
- 3: Korea University of Science and Technology, Daejeon, South Korea.
- 4: National Institute of Communications and Technology, Koganei, Tokyo, Japan.
- 5: Department of Arctic Geophysics, The University Centre in Svalbard, Norway.

**Contents of this file**

Figures S1 and S2

**Introduction**

Figure S1 shows the improved REProduce Plasma Universe (REPPU) simulation results of the field-aligned current (FAC) map on the magnetic equatorial plane in the nightside magnetosphere and the distribution of the ionospheric conductance determined by the magnetotail conditions, that is, a proxy of the ionospheric FAC intensity. The simulation results at the nearest times when Polar observed the fine auroral spiral (one of the auroral spots seen at the poleward edge of the nightside auroral oval) and the contemporaneous appearances of the nightside distorted transpolar arc (J-shaped TPA) and the auroral spiral are shown. In Figure S2, the deviations of the two geomagnetic field components ( $B_E$  and  $B_Z$ ) and their power spectrograms at the three ground magnetometer stations on the Svalbard island which were located near the auroral spiral are shown to examine what perturbations (or waves) in an ultra-low-frequency band can be observed in association with the auroral spiral.

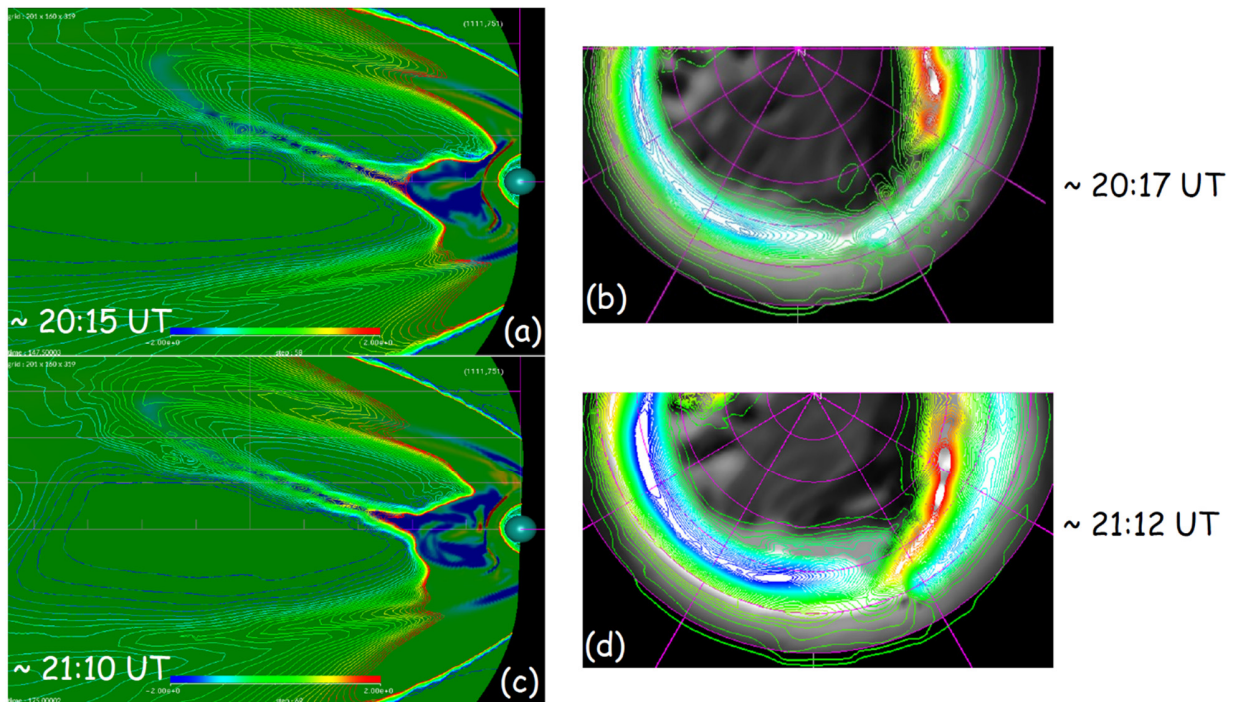


**Figure S1.** Snapshots of the results of the global MHD simulation, based on the improved REProduce Plasma Universe (REPPU) code (Tanaka, 1994; Nakamizo et al., 2009) when the auroral spots including the auroral spiral appeared at the poleward edge of the nightside auroral oval (~20:17 UT) and when the J-shaped TPA and the auroral spiral contemporaneously appeared (~21:10 UT) are shown. Panels a and c show the colored field-aligned current (FAC) contours projected on the magnetic equatorial plane. Panels b and d show the auroral conductance (a proxy of the FAC intensity, color contours) in the nightside ionosphere from 18 h to 6 h MLT at the nearest times of panels a and c.

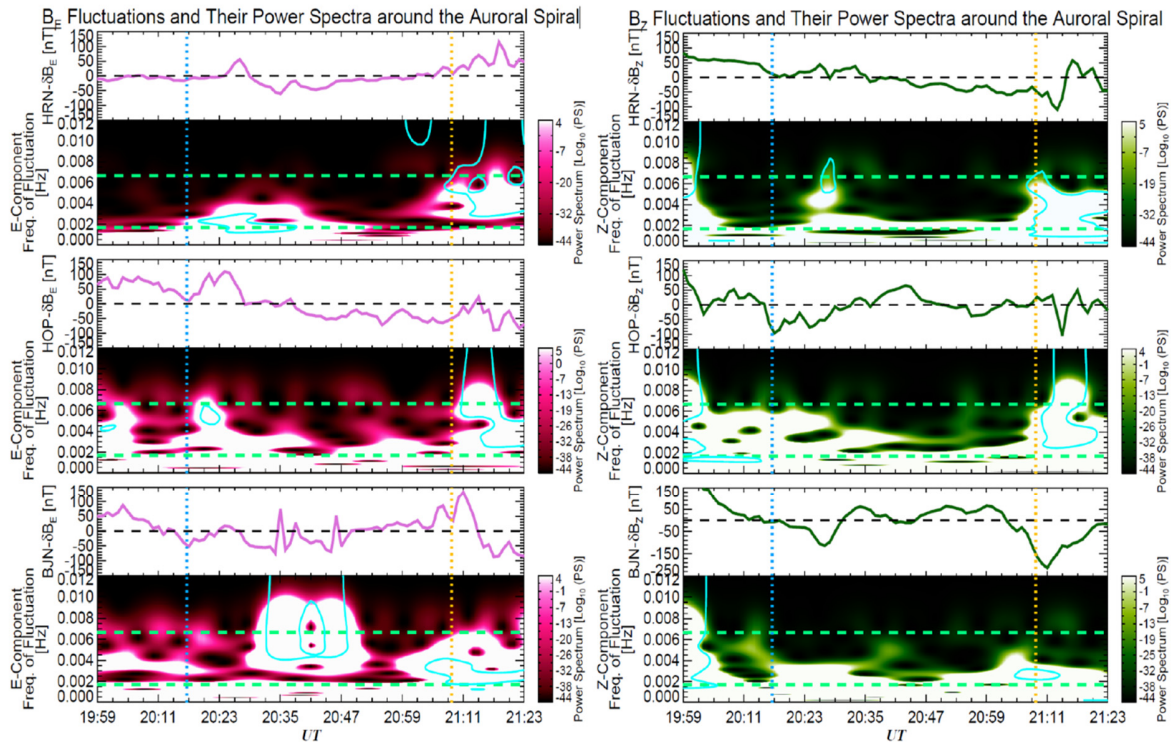


**Figure S2.** Deviations of the  $B_E$  (local magnetic east–west direction) and the  $B_Z$  (vertical up–down direction) components and their power spectrograms at the HRN (HOR), HOP, and BJN stations during the time intervals of auroral spiral on and near the Svalbard island from 19:59 to 21:23 UT are shown. The power spectra of these geomagnetic field fluctuations were calculated, based on the wavelet analysis using the Morlet function (Torrence and Compo, 1998). The vertical axis gives the frequency of the AC components of  $B_E$  and  $B_Z$ , and the color code is assigned to the logarithmic values of the wave power intensity. The confidence level higher than 93% for the wave power intensity is surrounded by cyan solid curves. The frequency range of Pc5 waves (1.67 – 6.67 mHz) are bracketed by two horizontal green broken lines. The two times of interest of 20:16:32 UT (fine auroral spiral) and 21:08:40 UT (contemporaneous appearances of the J-shaped TPA and auroral spiral) are indicated by sky blue and orange vertical broken lines, respectively.